6-2022

THE INTERACTIVE SIMULATION OF MARS DUST STORMS WITH THE MARS GENERAL CIRCULATION MODEL MARSWRF AT THE RESOLUTION OF 7.5°×9° (LATITUDE BY LONGITUDE)

Khulood Hasan Alshehhi

THE INTERACTIVE SIMULATION OF MARS DUST STORMS WITH THE MARS GENERAL CIRCULATION MODEL MARSWRF AT THE RESOLUTION OF 7.5°×9° (LATITUDE BY LONGITUDE)

Khulood Hasan Alshehhi

June 2022

United Arab Emirates University
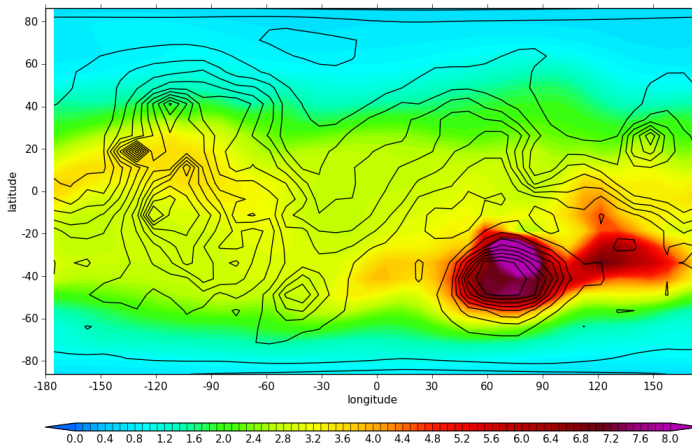
College of Science

Department of Physics

THE INTERACTIVE SIMULATION OF MARS DUST STORMS WITH THE MARS GENERAL CIRCULATION MODEL MARSWRF AT THE RESOLUTION OF 7.5°×9° (LATITUDE BY LONGITUDE)

Khulood Hasan Alshehhi

This thesis is submitted in partial fulfilment of the requirements for the degree of Master of Science in Physics

June 2022

Cover: A plot of the Dust Optical Depth for the sol 555 with solar longitude of 294.491 In the Martian Year 4 for the $7.5° \times 9°$ (latitude by longitude) model run.
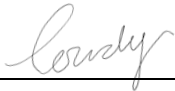
(Photo: by Khulood Alshehhi)

Declaration of Original Work

I, Khulood Hasan Alshehhi, the undersigned, a graduate student at the United Arab Emirates University (UAEU), and the author of this thesis entitled "*The Interactive Simulation of Mars Dust Storms with the Mars General Circulation Model MarsWRF at the resolution Of 7.5°×9° (latitude by Longitude)*", hereby, solemnly declare that this thesis is my own original research work that has been done and prepared by me under the supervision of Dr. Roland Young, in the College of Science at UAEU. This work has not previously formed the basis for the award of any academic degree, diploma or a similar title at this or any other university. Any materials borrowed from other sources (whether published or unpublished) and relied upon or included in my thesis have been properly cited and acknowledged in accordance with appropriate academic conventions. I further declare that there is no potential conflict of interest with respect to the research, data collection, authorship, presentation and/or publication of this thesis.

Student's Signature: _____

Date: ___23/Jun/2022_____

Advisory Committee

1) Advisor: Dr Roland Young

Title: Assistant Professor

Department of Physics

College of Science

2) Co-advisor: Dr. Claus Gebhardt

Title: Postdoctoral Fellow

National Space Science and Technology Center

Approval of the Master Thesis

This Master Thesis is approved by the following Examining Committee Members:

1) Advisor (Committee Chair): Dr Roland Young
   Title: Assistant Professor

   Department of Physics

   College of Science

   Signature _____   Date ___23 June 2022___

2) Member: Dr Abdelgadir Abuelgasim

   Title: Associate Professor

   Department of Geography and Urban Sustainability

   College of Humanities & Social Science

   Signature _____   Date ___10 June 2022___

3) Member (External Examiner): Dr Christopher Lee

   Title: Assistant Professor

   Department of Physics

   Institution: University of Toronto, Ontario, Canada

   Signature _____   Date ___13 June 2022___

This Master Thesis is accepted by:

Dean of the College of Science: Professor Maamar Benkraouda

Signature _Maamar Benkraouda_

Date August 25, 2022

Dean of the College of Graduate Studies: Professor Ali Al-Marzouqi

Signature Ali Hassan

Date August 25, 2022

Abstract

The Mars dust cycle, including dust storms, have a great impact on the temperature, and the climate in general, on Mars. Dust particles in the atmosphere have a great capacity of absorbing/emitting infrared radiation resulting large change in the Martian climate. Local and regional dust storms occur in any Martian Year (MY), but global dust storm events (GDEs), that can cover the whole planet, occur, on average, once every 3-4 MYs. MarsWRF is a Mars version of the terrestrial numerical weather and climate model WRF (Weather Research and Forecasting Model) and part of the PlanetWRF models for planetary atmosphere research. This requires model calibration by trial and error. The main focus is the formation of global dust storm events. The technique is to run MarsWRF in interactive dust mode. This requires the model user to self-specify the model parameters of the surface dust lifting by dust storms and dust devils. In this thesis the MarsWRF model is run in interactive dust mode at the classical resolution of $7.5°\times9°$ (latitude by longitude). The resulting dust storms will be compared against higher resolution simulations in Gebhardt et al. (2020).

Keywords: Mars, Atmosphere, Dust, Dust Cycle, Global Dust Storm events, Dust Devils, MarsWRF, Mars General Circulation Model (MGCM).

Title and Abstract (in Arabic)

المحاكاة التفاعلية للعواصف الرملية المريخية مع نموذج الدوران العام للمريخ MarsWRF

بدقة 9° × 7.5° (خطوط الطول بدوائر العرض)

الملخص

تعتبر دورة الغبار ذات أهمية أساسية للغلاف الجوي للمريخ. فهي محرك رئيسي للتغير بين السنوات للغلاف الجوي المريخي. بينما تحدث العواصف الرملية المحلية والإقليمية في أي سنة مريخية (MY)، تحدث أحداث العواصف الرملية المريخية (GDEs)، في المتوسط، مرة واحدة كل 3 - 4 سنوات (كما هو معروف، سنة مريخية واحدة تساوي حوالي 1.9 سنوات أرضية). MarsWRF هو نسخة خاصة بالمريخ من نموذج الأرض للطقس والمناخ WRF (نموذج أبحاث الطقس والتنبؤ) وجزء من نماذج PlanetWRF لأبحاث الغلاف الجوي. مثل أي نموذج دوران عام للمريخ (MGCM)، فهو مصمم لمحاكاة الغلاف الجوي للمريخ للعديد من السنوات المريخية. يكمن التحدي في إعداد MarsWRF لإنتاج محاكاة للعواصف الرملية المريخية (GDEs) في عدد قليل من السنوات المريخية فقط وليس كلها. تحقيقا لهذا، هناك تقنية متطورة تعمل على تشغيل MarsWRF في ما يسمى وضع الغبار التفاعلي. وهذا يعني أن غبار المريخ يُرفع بحرية تامة عن السطح، وينتقل عبر الغلاف الجوي، ثم يترسب مرة أخرى على السطح. وينتج النموذج عواصف المريخ بشكل مستقل. وهذا يتطلب من المستخدم أن يحدد ذاتيًا قيم رفع الغبار السطحي عن طريق العواصف الرملية والدوامات الترابية. يتم تحديد قيم المعلمات المثلى من خلال التجربة والخطأ. نظرًا لأن تأثير القيم يعتمد على دقة النموذج والإعدادات الأخرى، يجب إجراء النموذج بشكل فردي. يتم تقييم أداء النموذج من خلال مقارنات بين درجة حرارة الغلاف الجوي المتوسط للمريخ بين النموذج وسجل رصد الأقمار الصناعية التي تدور حول المريخ. تتمثل مهمة هذه الاطروحة في تشغيل نموذج MarsWRF في وضع الغبار التفاعلي ب بدقة 9° × 7.5° (خطوط الطول بدوائر العرض). سيتم استكشاف العواصف الرملية الناتجة ومقارنتها بدقة أعلى في بحث (Gebhardt et al., 2020).

مفاهيم البحث الرئيسية: المريخ، الغلاف الجوي، الغبار، دورة الغبار، العواصف الرملية المريخية، سنة مريخية، نموذج الدوران العام للمريخ.

Author Profile

I am Khulood Alshehhi, a Master student in the Physics department at United Arab Emirates University (UAEU) under the supervision of Dr. Roland Young, since August 2020. I am also a part-time Research Assistant and an MSc studentship holder at the National Space Science and Technology Center (NSSTC) with Dr. Claus Gebhardt, UAE University. My work at the NSSTC is a crucial part of my MSc and has allowed me to acquire knowledge and practical experience in Space Science as well as to fulfill the thesis requirement of the Master's degree. My work at the NSSTC focusses on Mars dust storms and Mars surface and atmosphere.

As part of my Master's degree work, I participated in December 2021, as the first author of a poster, in the AGU conference in New Orleans, LA, USA. The poster was titled "*Comparing dust storm simulations at horizontal model resolutions of 5°×5° and 7.5°×9°, based on the interactive dust lifting technique*".

I obtained a Bachelor of Science degree in Physics from UAEU in June 2020. During my undergraduate studies, I participated in several conferences and workshops. In July 2019, I participated in the Ninth International Conference on Mars at the California Institute of Technology (Caltech) in Pasadena, CA, USA. The undergraduate research project was on Mars water-ice-clouds with the title "*visual analysis of spatiotemporal variations of Mars ice clouds using MARCI data*". In March 2019, I took part in the Global space congress in Abu Dhabi with a poster presentation about "*Visual Analysis of Spatiotemporal Variations of Ice Clouds on Mars*".

Acknowledgements

Dedication

To my beloved granny,

Fatma Hasanat

Table of Contents

List of Tables

List of Figures

List of Abbreviations

AB	Argyre Basin
AM	Alba Mons
AP	Amazonis Planitia
AT	Arabia Terra
CDOD	Column Dust Optical Depth
CTA	Coupling Term Acceleration
DCI	Dust Cover Index
EDDLs	Extremely Detached Dust Layers
EM	Elysium Mons
ESA	European Space Agency
GCM	General Circulation Model
GCM	Global Climate Model
GDEs	Global Dust Storm Events
GFDL	Geophysical Fluid Dynamics Laboratory
HB	Hellas Basin
HP	Hesperia Planum
MarsWRF	Mars Weather Research and Forecasting Model
MGCM	Mars General Circulation Model

MGS   Mars Global Surveyor

MOLA   Mars Orbiter Laser Altimeter

MY   Martian Year

NASA   National Aeronautics and Space Administration

NCAR   National Center for Atmospheric Research

OM   Olympus Mons

TES   Thermal Emission Spectrometer

TM   Tharsis Montes

TR   Tharsis Rise

TT   Tempe Terra

VM   Valles Marineris

WRF   Weather Research and Forecasting Model

Chapter 1

Chapter 1: Introduction

1.1 Overview

In this thesis, I studied the phenomena of global dust storm events (GDEs) on Mars using the model MarsWRF. This model is the Mars version of the Weather Research and Forecasting Model (WRF) and is part of the PlanetWRF. It is designed to simulate the Martian atmosphere for many Martian years (MYs), just as any other Mars General Circulation Model (MGCM). One major problem is to set up MarsWRF to Produce GDEs in a few MYs, but not in others. This first chapter will introduce the Mars atmosphere, the dust cycle and previous relevant literature. The second chapter discusses the model MarsWRF and how it works. Finally, the last chapter shows the result for the optimal model run and its comparison with higher resolution model runs.

1.2 Statement of the Problem

Global dust storms only occur intermittently on Mars. Whereas local and regional dust storms happen every year, Global dust storm events that can cover the whole planet only occur once every three to four Martian years. The challenge then is to set up the model MarsWRF to produce Global storm events (GDEs) only in some Martian years but not all of them.

1.3 Research Objectives

Local and regional dust storms show in any Martian year, but Global Dust Storm events (GDEs) only appear on average every 3-4 MYs. In this research, we study the phenomena of Global Dust Storms that occur on Mars using the model MarsWRF. More specifically, we run the model in interactive dust mode at the classical resolution of 7.5°×9° and compare it with the Existing model data at the higher resolution of 5°×5°.

1.4 Literature Review

The dust cycle is an essential component, and one of the major drivers, of the Martian climate. In suspension in the atmosphere, dust absorbs, reemits, and scatters solar radiation. This, in turn, has a major impact on the temperature, both on the surface of the planet and in its atmosphere. The dust cycle has also a crucial influence on the dynamics of the Martian atmosphere (Levine et al., 1977). Much research has been done on Martian dust cycle and storms and their nature.

It was found that the dust cycle on Mars shows variations in one year time or less than a year. This yearly change is the result of the Martian hemispheric dichotomy in topography. The result shows that around perihelion, when the summer or spring season occurs in the southern hemisphere, the atmosphere of Mars becomes warm and dusty. Along with this, the Southern hemisphere is elevated higher, thus resulting in global circulation leading to dust lifting. Similarly, around the aphelion, atmospheric dust is scarce; typically, local dust storms are witnessed here. Global dust storms do not occur here. However, local and regional dust storms occur yearly, whereas global dust storms occur on average once every few Martian Years.

Volcanic formations, such as those shown in Figure 1 and related topography have an extremely important effect on wind and dust circulation. Volcanoes and their slopes have been shown to serve as a launching pad for water vapor and dust from the surface high into the atmosphere (Heavens et al., 2015). Observations for the Mars Reconnaissance Orbiter show dust layers high in the atmosphere, often more than 1000 km wide, clustered around Olympus Mons and the Tharsis Montes. The assumption is that they originate from these volcanic formations (Heavens et al., 2015).
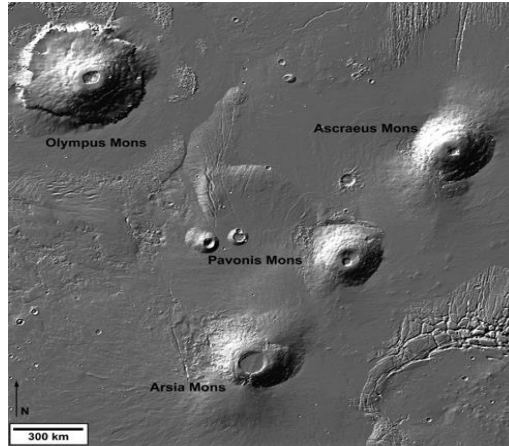
Figure 1: Volcanoes (Olympus Mons, Ascreaus Mons, Pavonis Mons and Arsia Mons) - NASA (2007)

These dust layers above an altitude of 50 km are called extremely detached dust layers (EDDLs). Their study requires mesoscale models with a horizontal resolution of around 10 km. Our work, however, is not on these EDDLs but on large dust storms. Although there are some similarities between Mars and the Earth's dust storm generation, many unrevealed mysteries lie beneath Mars' dust particles (Zurek et al., 1992).

In this thesis, we use some abbreviations such as HB for Hellas Basin. Figure 2 shows a map produced by NASA, using The Mars Orbiter Laser Altimeter (MOLA) data through October of 2000. The map has a very high resolution topographic shaded relief with the name of the regions (NASA, 2000b).
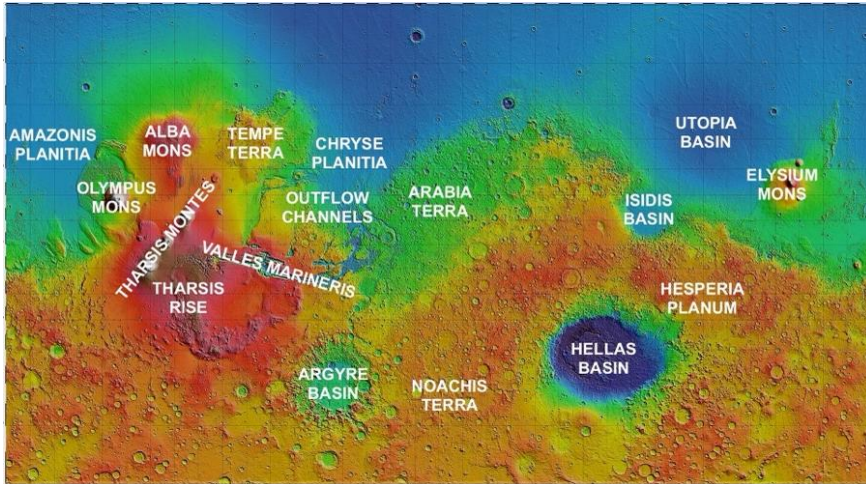
Figure 2: Using MOLA data through October of 2000, the Science Team has produced a very high resolution topographic shaded relief map of Mars (NASA, 2000b)

1.4.1 Dust Storms Formation

During the day, the airborne dust particles are raised from the surface into the atmosphere due to the heated Martian surface by sunlight. These dust particles heavily depend on the development of wind circulation above a couple of kilometers of surface called the planetary boundary layer (Kahre et al., 2017). The strong dusty winds absorb sunlight radiation and produce a thermal infrared wavelength that can be detected (Petrosyan et al., 2011). A complete understanding of Mars's atmospheric activities requires a deep knowledge of seasonal transport and dust removal and other elements such as CO_2 and water vapor (Wu et al., 2021).

1.4.2 Dust Storms Activity on Mars

Local and regional dust storms are common every Martian year. However, larger global dust storms only occur every 3 to 4 Martian years (Zurek & Martin, 1993) and they can cover large areas, as shown in Figure 3 for the Thaumasia region on Mars.
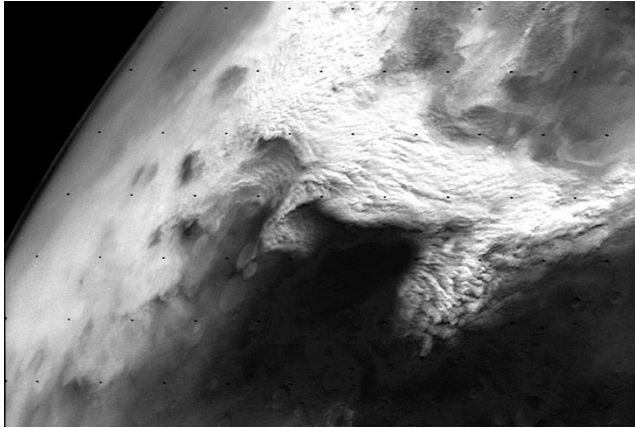
Figure 3: This Viking Orbiter 2 image shows a large dust storm over the Thaumasia region on Mars. This large disturbance soon grew into the first global dust storm observed by the Viking Orbiters (NASA, 2018)

On Mars, dust storms may grow to global size and have a duration of up to a few months. It has also been found that the Martian global dust storm can completely hide the planet with haze in a couple of weeks. Such global dust storm events (GDEs) are irregular in time and occur in few but not all Martian Years (MYs) (Zurek & Martin, 1993). On average, one GDE occurs each 3-4 MYs (1 MY is equivalent to 1.9 Earth Years). The last GDE took place in Earth Year 2018. Before, there were also GDEs in 2007 and 2001 e.g. (Forget & Montabone, 2017).

Although dust storms may grow to encircle the whole planet, they mostly originate from the regions of Acidalia, Utopia, Arcadia Planitia and

Hellas (Wang & Richardson, 2015). Other regions of Mars also experience major dust storms. For instance, Battalio & Wang (2019) focus their attention on dust storms in the southern hemisphere regions of Aonia-Solis-Valles Marineris. Dust activity in this region is the most important outside the dust storm season. It can affect the whole Martian atmosphere and has consequences that extend well beyond the region (Battalio & Wang, 2019).

In Battalio & Wang (2021), the authors investigate the concept of dust storm sequences, defined as a collection of dust storms that have a coherent trajectory from their area of origin during three to four sols. They found that the northern hemisphere sequences mostly originate in Acidalia, Utopia and Arcadia Planitia. In contrast, in the southern hemisphere, the areas of origin are mostly Aonia-Solis Valles Marineris and the Hellas Basin (Battalio & Wang, 2021).

The Martian low dust loading season stretches from $L_s = 0°\text{-}10°$ to $L_s = 140°$, during which the dust slowly dissipates, and very little dust lifting occurs. The period from $L_s = 140°$ to $360°$ is the high dust loading season as shown in Figure 4. This is the period when regional dust storms and global dust events are most likely to occur (Forget & Montabone, 2017).
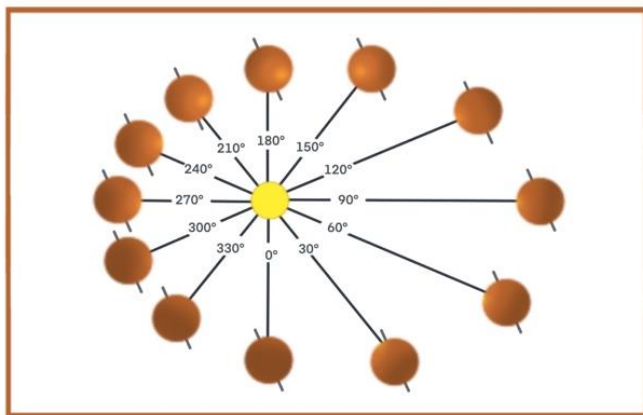
Figure 4: Mars solar longitudes

1.4.3 Nature of Martian Dust Storms

The GDE in 2018 was another demonstration that dust storms are critical to any infrastructure on the surface and in the atmosphere of Mars. During this GDE, contact with the Mars rover Opportunity was lost, and this mission came to an abrupt end after being in operation since 2004. Many studies, such as Bertrand et al. (2020), were carried out to better understand that particular dust storm and, by extension, a better understanding of general global dust storms. The study shows the main driver of the storm was a quick back and forth transfer of dust between eastern and western hemispheres' dust reservoirs (Bertrand et al., 2020).

Our knowledge of Mars dust storms is based on observations by Mars satellite orbiters, surface landers and rovers, Earth and space-based telescopes, numerical models, laboratory experiments, and Earth-Mars analogues. Figure 5 shows a Martian dust storm captured by NASA's Curiosity rover.
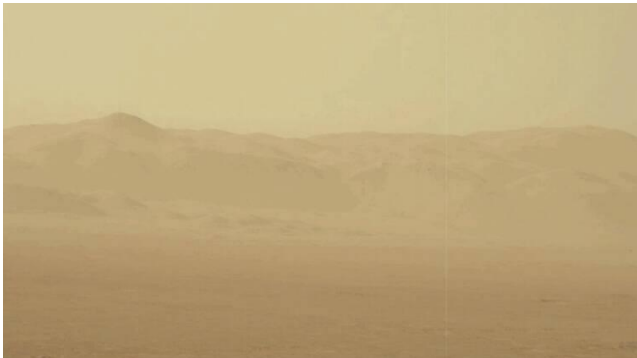
Figure 5: Martian dust storm captured by NASA's Curiosity rover

1.4.4 Modelling of Martian Dust Cycles

Despite extensive research, dust storms on Mars remain difficult to understand, predict or simulate with great accuracy (Newman et al., 2021). Their scarcity (there have only been 10 GDEs since observation began in 1956) makes them particularly difficult to study and simulate.

Running a Mars climate model with "interactive dust" accounts for dust processes such as dust lifting, transporting and depositing. Lifting is usually achieved by surface wind stress or by dust devils. Airborne dust affects the temperature, the wind, and the atmosphere's radiative properties. These, in turn, provide strong feedback on the dust lifting process (Newman et al., 2021).

Initially, Martian simulation models assumed unlimited dust availability. The results of these simulations often did not match observation. Later models assumed limited dust availability. Here too, the results were often unrealistic (Newman & Richardson, 2015). The latest model incorporates both dust and water cycle the result still do not entirely match observation (Lee et al., 2018). Producing reliable models will require a better understanding of dust and sand motion on Mars. A precise simulation of the physical conditions prevailing on Mars is also crucial to any model (Newman et al., 2021).

A global numerical model known as a General Circulation model (GCM) integrates the primitive equations of atmospheric motion and a range of other physical constraints and 'forcings' to yield a simulation of the global atmosphere and the global climate. GCMs have been applied to various planetary atmospheres since the 1960s (Leovy & Mintz, 1969), not long after their introduction into terrestrial atmospheric science. Mars General Circulation Model (MGCM) is commonly used to model Martian

atmospheric circulation. The use of these models for global-scale modelling started almost half a century ago (Toigo et al., 2012) These models proved best in explaining the emission, nature, and timing of dust storms on Mars. Much research has been done on Mars General Circulation Models with different parameters. For our work, it is important that both $5° \times 5°$ and $2° \times 2°$ resolutions show a certain degree of concordance with observation-based dust cover maps. Richardson et al. (2007) worked on a planetary model derived from NCAR WRF (National Center for Atmospheric Research, Weather Research and Forecasting model). Detailed mathematical description concerned with specific changes to the dynamical core is provided. The paper provided enough results to show that this model works well for application on several scales to Mars at various global scales.

Newman et al. (2019) present the first Mars General Circulation Model (MGCM) simulations of a fully interactive dust cycle with the inclusion of Coupling Term Acceleration (CTA) to predict dust storm sizes, onset times and locations. The inclusion of the CTA increases the model's skill at forecasting global dust storms and non-global dust storm Martian Years (MY) compared to an MGCM without CTA forcing. Their model is mostly accurate in capturing the general onset time of most observed storms and some onset locations while proving wrong in only 4 out of 22 well-observed storm seasons.

Mismatches in the model (early GDEs are observed but not predicted in two MYs (12 and 25)) occur due to a lack of water cycle coupling, missing physical processes, and the assumption of unlimited surface dust availability, and imperfect parameter values, or the wrong CTA strength. The model correctly predicted the global dust storms close to perihelion in the storm season, MY34 (2018), while a smaller global dust storm was predicted later next Mars year, i.e. MY35 (2020). The CTA

forcing in MY 34 is very similar to that of MY 21, in which a global dust storm is correctly predicted by the model.

Bertrand et al. (2020) conducted their study to understand the evolution of the global dust storm event created on Mars in June 2018. They modelled the event with the National Aeronautics and Space Administration (NASA) Ames Mars Global Climate Model. The finding shows that global dust storm is characterized by rapid eastward transport of dust in the equatorial regions and subsequent lifting. Large dust plumes occur during the mature phase, injecting dust up to 80 km. Another important finding is that the height at which water condenses increases during storms, resulting in more water vapors in the upper atmosphere.

Basu et al. (2006) simulate global dust storms by applying Mars global circulation model (MGCM). The simulated storms used in the model are developed on multiyear simulations and exhibit inter annual variability. Their observations support the idea that for the emergence of a variable and spontaneous global dust storm behavior from a periodically forced system, a dust injection mechanism through threshold activation is needed. Their simulation storm is initiated by surface wind stresses associated with resolved large scale (>300) wind systems. These winds are linked with Hellas basins' seasonally migrating CO_2 cap boundary, travelling waves and thermal tides. A few large storms are initiated with lifting along the frontal zones linked with travelling waves in the northern hemisphere.

Liu (2003) conducted a study that focuses on air temperatures, dust opacities and water ice opacities from thermal infrared data collected by Mariner 9, Viking, and Mars Global Surveyor (MGS) to reduce inter-instrument biases and offsets, emphasis is placed on creating a uniform data set. During northern spring and summer, the annual cycle constantly shows strong irregularity about the equinoxes, with averaged Martian nighttime air

temperatures close annually to within a Kelvin. In contrast, Daytime temperatures show more variability (3–6 K). The difference in temperatures is not understood. Viking and MGS eras are categorized by essentially the same climatic state. Southern summer is characterized by strong dust storm activity, responsible for yearly temperature variability. However, late northern spring and early northern summer dust opacities appear to be completely unresponsive to the incidence (or not) of dust storms in the former southern spring or summer. Viking and MGS data sets exhibit similar polar cap edge dust storm activity, and thermal infrared data from Viking and MGS proves very helpful in detecting the origin of major dust storms. It is noted that the period around $L_s = 225^o$ is described by very high dust opacities which is related to storm development. Viking infrared data is proved very fruitful in retrieving Water ice opacities. Overall observations reveal that the Martian atmosphere is filled with some repeated annual cycle atmospheric phenomena, where occurrences of many potential dust storm events are its major parts. However, after such dust storm events, the atmosphere quickly regains its stable and repeatable state.

Forget et al. (1999) derive two new generation GCM of the Martian atmosphere based on their previous model developed in the 1990s. These models share the same physical parameterizations, but in order to solve atmospheric dynamic equations, two complementary numerical methods are used. With refined vertical resolution surface and up to 80 km extended vertical domain and state-of-the-art parameterizations, simulation of dynamical and physical processes near the surface and at high altitudes is best proven by these models. By testing the model at several seasons, examples of zonal mean fields are presented, indicating that the representation of polar processes has been improved significantly. The winter polar warming introduced by Wilson (1997) had been detected but

not properly modelled until recently, but this model predicted the thermal inversions of poles around 60-70 km. However, Mars's middle atmosphere above 40 km is difficult to stimulate accurately in the absence of observations because it is found to be very model-sensitive. Jakosky et al. (2000) determined the thermal inertia of the Martian surface up to 100 km spatial scales by using Mars Global Surveyor Thermal Emission Spectrometer. In order to derive thermal inertia, they included only nighttime measurements along with single wavelength band versus bolometric thermal emission measurements.

Guzewich et al. (2013) forced Mars WRF GCM using two versions of dust climatology developed from 3 Mars years of TES Limb-scanning Figure 6 dust observations examined the results to analyze the impact of vertical dust profile on thermal tides, the general circulation of the atmosphere and planetary waves. Their finding shows that the vertical dust profile is a key factor of atmospheric forcing on Mars. Observations from TES, along with MCS retrievals, indicate that specifically for low latitudes, the traditional and modified Conrath-ν vertical dust profile does not precisely represent the true vertical dust profile, and many of the features of Martian climate, including the polar warmings, Hadley circulation, and thermal tides are internally controlled by vertical dust profile (Guzewich et al., 2013).
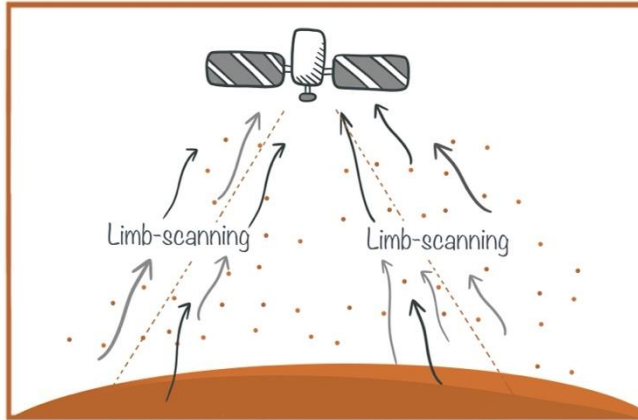
Figure 6: The absorption and scattering of the infrared radiation of TES Limb-scanning

Basu et al. (2004) suggest that there is a strong relationship between the dust distribution, the atmospheric circulation and heating rates that helps in the transportation of the dust from one place to another and, therefore, in the creation and sustainability of dust cycles. They used the Geophysical Fluid Dynamics Laboratory (GFDL) Mars GCM model to address the questions related to dust storms. Their GCM simulation of interactive dust cycle results help explain whether the injection schemes can generate a dust cycle and what combinations of parameters show the best fit. The dust injection scheme used in this study includes detailed, physical-based parameterizations of dust lifting particles. Parameters used are rate constants applied to two injection schemes and threshold lifting stress. Findings from the model help in predicting those dust devils are the primary dynamical system providing the dust injection essential to sustain the Mars background haze. Also, dust storms cannot be generated in the model, supporting the point that dust devils are not the originators of the dust storms. The distribution and seasonal variation of dust devil activity are also predicted.

However, a comparison of air temperatures across section data proposed that cap edge lifting is unpredictable. The most important fact is that this model is best for predicting the rate of dust injection and the net deposition of dust on the surface.

Newman et al. (2002) examined the suspended dust distribution obtained using various lifting parameterizations by implementing the Mars General Circulation Model (MGCM). The model uses multiannual dust transport simulations based on dust transport schemes that respond to the atmospheric state changes. Two lifting mechanisms are selected, i.e. near-surface wind stress and dust devils. Each mechanism is divided into two types of parameterizations: threshold-sensitive and -insensitive. Results show that threshold-sensitive parameterizations are better in producing more realistic annual and inter-annual behavior, proposing an insight into how real Martian dust storms may develop. Simulations for which dust devil lifting dominates are too dusty during northern summer, suggesting that dust devils are not the primary mechanism for storm production. The seasonal state of the atmosphere is closely related to simulated dust levels, and hence no simulation produces the observed amount of inter annual changeability.

Running any MGCM has considerable computational requirements. For MarsWRF, the optimal computation speed is achieved when employing a supercomputer with more than 100 processors (Laux et al., 2013). The total computational load of a model simulation strongly depends on the used model resolution in terms of latitude, longitude, and altitude.

1.4.5 MarsWRF Model with Interactive Dust

A particular challenge for MGCMs is to correctly simulate the occurrence of GDEs in a few MYs but not in others, known from observations. To this end, a sophisticated technique is given by running the

MarsWRF model with interactive dust parametrization (I.D.). This means that dust is completely freely lifted from the surface, transported through the atmosphere, and deposited back onto the surface Figure 7. And dust storms are self-consistently produced by the model. This requires the user to self-specify the surface dust lifting model parameters by dust storms and dust devils. The optimal parameter values are determined by a trial-and-error approach. As the effects resulting from such parameter values depend on the model resolution and other settings, this model calibration must be done individually for any model configuration. While some studies used interactive dust other modeling studies used prescribed dust. Whatever the model used its performance is evaluated by comparisons against observational data, such as the Martian midlevel atmospheric temperature. Some studies use Interactive dust, whereas many modelling studies use prescribed dust (Guzewich et al., 2013).
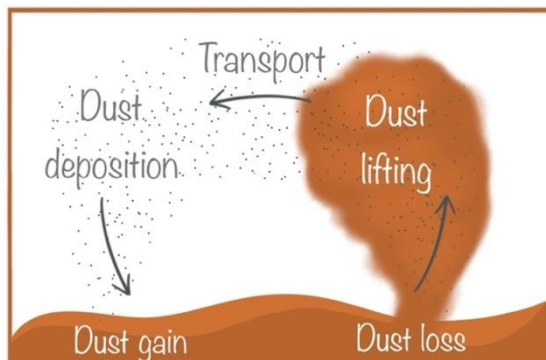
Figure 7: The process of interactive dust: the dust is lifted from the surface, transported, and then falls back to the surface

Newman & Richardson (2015) apply MarsWRF GCM to examine the impact of the finite and infinite surface dust cover on the Martian dust cycle by interactive dust. They tried to find a long-term 'steady state' dust

cycle for present-day Mars, based on surface dust distribution that fluctuates from year to year but remains constant in a longer-term and fixed set of dust lifting parameters that endure yielding major storms for this distribution of surface dust. Their result demonstrates that the GCM exhibits quasi-steady-state behavior with constant dust lifting parameters while few new surface grid points are exhausted during a 60 year period. For many realistic features, including merging regional storms, cross-equatorial storms, and the timing and location of several storm types, GCM generates regional to global dust storms. The finding shows that early major storms are onset by surface dust availability, while regions where storms prevailed before depend on atmospheric variability for another storm to occur. As per the parameter space explored, no simulation achieves a steady-state for storms during the 60 year period when a constant wind stress lifting threshold is used. Though, such a long-term steady-state is attained when a variable threshold is introduced, in which the threshold increases as dust is removed. One concern is that their long-term surface distributions produced in these simulations show differences from one observed in the northern hemisphere albedo map predicting Tharsis and NE Arabia to be relatively dust-free. These discrepancies may be because of shortcomings in the GCM, the iterative process used, or the ancient deep dust deposits prevailing during the past climate epochs.

1.4.6 MarsWRF Resolution.

Gebhardt et al. (2020) set up the Mars WRF and MGCM using "interactive dust", which states that the model freely lifts, transports, and deposits surface dust. They use two horizontal model grid point resolutions of $2° \times 2°$ with 45 vertical levels and a $5° \times 5°$ resolution and compare their results in terms of changes in surface dust loading and dust storm source regions. This was the first time the model was set up with $2° \times 2°$. Resolution

and interactive dust. While Newman & Richardson (2015) also set up the model in interactive dust mode, their resolution was much closer to $5° \times 5°$ resolutions. While configuring their interactive dust, Gebhardt et al. (2020) use three parameters: the dust devil lifting rate constant αD (kg/J), the wind stress lifting threshold τ (Pa), and the wind stress lifting rate constant αN. Their findings show that for high resolution of $2° \times 2°$, GDEs are likely to occur if regional dust storm activity in the northern Hellas basin and south of Chryse Planitia (equatorial source regions on the planet) combine with one another. Another important aspect is that the model's surface dust distribution in the case of a high-resolution experiment agrees potentially better with observation-based dust cover maps.

Chapter 2

Chapter 2: Methods

2.1 The Development of the MarsWRF Model

In order to understand the Martian atmosphere and its dust cycle, observations and numerical modelling are both of vital importance. Observations provide information regarding the presence of dust in the atmosphere, and the time, location, and magnitude of the dust storms. Through observations, we can also determine the nature and composition of the dust as well as its effect on the temperature of the surface and the atmosphere. However, the forecasting of Mars dust storms is extremely difficult. On the other hand, numerical models can help understand how, where, and when dust enters the atmosphere. It can also help us understand how dust travels through the atmosphere and how it is deposited on the surface (Kahre et al., 2017).

The Planetary Weather Research and Forecasting model (PlanetWRF) is a model for numerical simulation that can be used for research into the weather, atmosphere, and climate systems of various planets. This model was developed by modifying the Weather Research and Forecasting (WRF) model, which was developed at the National Center for Atmospheric Research (NCAR) (Richardson et al., 2007).

WRF could be run on supercomputers such as the NASA Pleiades supercomputer. WRF was used primarily in research into Earth atmospheric phenomena, including weather forecasting. However, WRF capabilities were somehow limited. WRF was not a comprehensive modelling system for two reasons. Initially, it was impossible to simulate a fully global domain, and it was written to be used exclusively on Earth.

Three main modifications were applied in order to transform the original WRF into a planetary WRF. These modifications were then applied

back into the EarthWRF to finally result in PlanetWRF. They were primarily in the domains of non-conformal map Projections, Polar Boundary Conditions and Generalized Planetary parameters and calendars. PlanetWRF is now being used for research into the atmospheres of Mars, Titan, Jupiter, Saturn, Pluto, and Venus (Richardson et al., 2007).

The MarsWRF has generalized map-projection, multi-scale and nesting capabilities which allow the elimination of the distinction between global, meso and micro-scale models. This allows the investigation of coupling between processes on all scales. MarsWRF domains can extend from a few hundred meters to thousands of km, and they can encompass very high-resolution domains within progressively lower-resolution domains on larger scales. The model can also run in one, two or three dimensions (Toigo et al., 2020). The present work was carried out using the global model in three dimensions.

2.2 The General Circulation Model for Planets

Every year, Mars experiences some dust storms. Local and regional dust storms may cover thousands of square kilometers and may last for days or even weeks at a time. There are also more massive and more intense storms that occur more rarely. Even more rare are massive global dust storms that may cover the whole planet, known as global dust storm events. More precisely, Martian dust storms were, until 2001, generally divided into three types (NASA, 2000):

1. Local dust storms are clouds and hazes with less than 2000 km spatial dimensions.
2. Regional dust storms are clouds and hazes that have spatial dimensions greater than 2000 km.

3. Global dust storms cover the whole planet at some latitude; see Figure 8, which shows the Global Dust Storm in 2018.
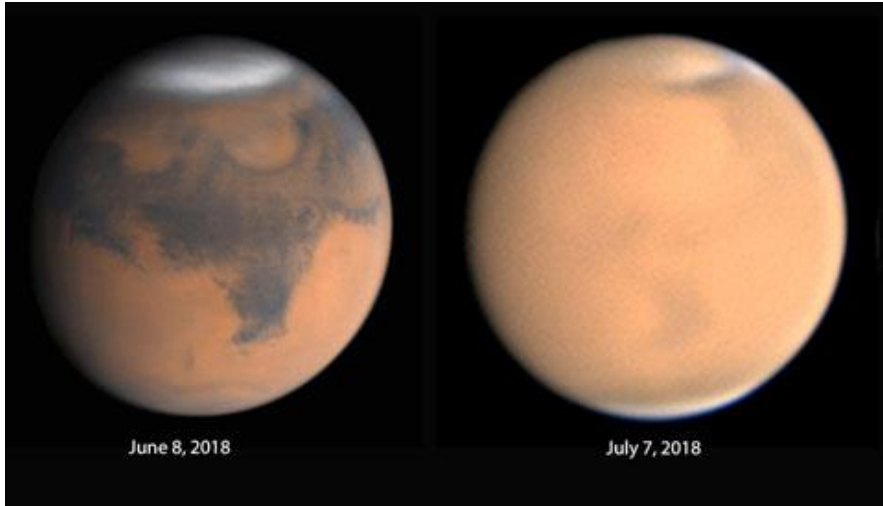
Figure 8: The same hemisphere of Mars, in one month in 2018. (left) with no global dust storm, (right) with global dust storm. Damian Peach/ Chilescope team (left), Christophe Pellier

In Cantor et al. (2001), dust storms are classified as local if they cover a surface from one hundred square kilometres up to 1.6 million square kilometres, and if having a duration of more than 2 days. Beyond this size, they are referred to as regional dust storms. If they cover the whole planet, they are global dust storms. Alternatively, Montabone and Forget (2018) define:

1. Local dust storms as storms that lefts dust particles over an area less than 1.6 million km^2 during less than three sols. This is just over 1% of the total Mars surface area.

2. Regional dust storms as storms that lefts dust particles over an area greater 1.6 million km^2 for between 4 and 20 sols.

3. Global dust events as a combination of several dust storms that last tens of sols and cover the whole planet.

Local and regional dust storms tend to occur in areas of high topographic and/or high thermal gradients (usually near the polar caps), where surface winds are the strongest. (Ho et al., 2002)

2.3 Wind Stress Saltation

Depending on the size of the particles and the speed of the wind, particles are moved and transported in several ways, as shown in Figure 9. One of these modes of transportation is known as saltation.

Saltation is the movement of particles along the ground by successive short distances. This ground bouncing leads to more particles being dislodged and, therefore, to the movement of increasingly more particles with each bounce. Saltation accounts for a relatively high proportion of soil dispersed by wind.
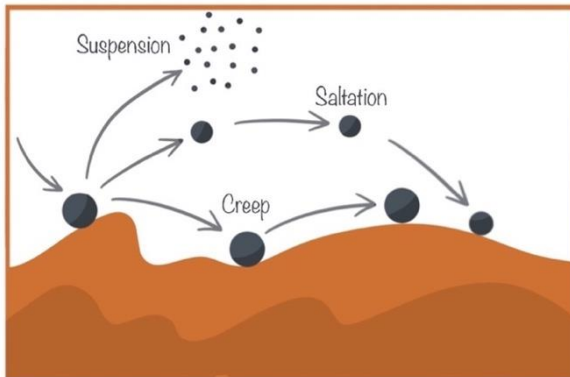
Figure 9: Wind transportation methods

Aeolian processes on Mars differ substantially from those on Earth, primarily due to large differences in gravity and air density. The lower air density makes it more difficult to move surface material on Mars. Still, dust storms are widespread, and evidence of active sand transport has been accumulating over many years (e.g., Bridges et al., 2012; Cantor et al., 2001).

In Newman et al. (2002a), the authors propose an equation for the minimum speed required for dust lifting to occur by wind stress:

$$u_{drag}^{t} = A \sqrt{g \, D_p \, \frac{\rho_d - \rho}{\rho}}$$

where A is a factor to be determined, D_p is the particle diameter (in meters), ρ_d is the density of the material from which the dust particles are made (approximately $2700 \, kg \, m^{-3}$). This equation is appropriate for Earth and other planets, including Mars. This formula confirms that larger particles (particles with larger D_p) are more difficult to lift. Factor A is found by solving a semi-empirical formula (Newman et al., 2002a).

2.4 Dust Devils

Dust devils are triggered when air rises, heated by the ground, and cooler air sinks towards the ground (see Figure 10). This creates vertical air circulation. If a wind blows through, the dust devil is formed. When spinning, the dust devil picks up dust and spreads it into the atmosphere and around the surface.

Dust devils on Mars can reach heights of eight kilometers, up to hundreds of meters wide and can travel several kilometers (ESA, 2022). They are a very important factor in the presence of dust in the atmosphere. According to some estimates, around 50% of the dust present in the atmosphere is lifted by dust devils (Haberle et al., 2006; Kahre et al., 2006; Raack et al., 2018; Whelley & Greeley, 2006). This makes them an important subject to study in understanding Mars' climate.
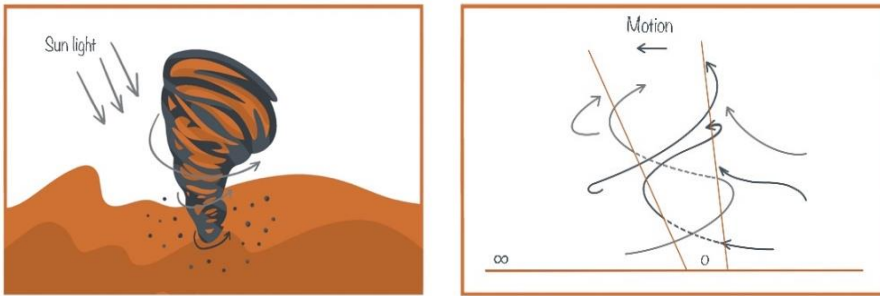
Figure 10: The dust devils form when the sun heats the surface and the hot air near the surface rises quickly through cooler air above it

Dust devils, whether on Earth or on Mars, present several characteristics. In Rennó et al. (1998), the authors show that:

1. There is a positive correlation between the intensity of a dust devil and the difference in temperature between the surrounding environment and the centre of the dust devil.
2. The temperature at the centre of a dust devil has an upper bound equal to the ground temperature.
3. Dust devils are more likely to form in an environment with large variations in ground-level temperatures.

4. The magnitude of the vertical component of the wind velocity within the dust devil can be calculated using the Renno & Ingersoll (1996) Equation:

$$w \approx \sqrt{\left(\frac{c_p}{8\epsilon\sigma_R T_C^3}\right)\frac{\eta F_{in}}{\mu}}$$

where $\epsilon \approx 0.7$ is the emissivity of the boundary layer air, $\sigma_R \approx 5.67 \times 10^{-8} \ W \ m^{-2} K^{-4}$ is the Stefan- Boltzmann constant, F_{in} is the heat input to the convective heat engine, and μ is a dimensionless coefficient of turbulent dissipation of mechanical energy.

2.5 Dust Devil as a Heat Engine

The thermodynamic efficiency η of a heat engine is defined as the fraction of the heat input that is turned into work. In Rennó et al. (1998) developed a model of dust devils as heat engines. In this model, it was shown that the amount of energy available to drive a dust devil is a function of two variables, namely the surface heat flux F_s, and the thermodynamic efficiency η, as shown in the following equation:

$$F = \eta \ F_s \ .$$

In this model, the authors also show that the thermodynamic efficiency η is approximated by:

$$\eta \approx 1 - \frac{p_s^{\chi+1} - p_{top}^{\chi+1}}{(p_s - p_{top})(\chi + 1)p_s^{\chi}}$$

Where;

- $\chi \equiv R/c_p$, where R is the specific gas constant for air, and c_p is the heat capacity at constant pressure per unit mass (specific heat capacity).
- p_s is the ambient surface pressure.
- p_{top} is the ambient pressure at the top of the convective boundary layer.

2.6 The Three Parameters Used in the Model

The use of parameters in MarsWRF greatly improves the accuracy and efficiency of the model. The parametrization allows for too complex processes to be included in the model to be replaced by simple processes. More specifically, parametrization is required for processes that the model cannot resolve. For example, dust devils cannot be resolved by a 2° x 2 ° or coarser resolution model because they have a diameter of not more than several hundred meters.

The first parameter, the dust devil lifting rate constant αD (kgJ^{-1}), is a constant of proportionality between the amount of dust lifted by dust devils per area and time, the surface sensible heat flux, and the PBL thickness. This parameter was set at 1.6×10^{-9} kgJ^{-1}

The second parameter is the wind stress lifting threshold τ (Pa), which is related to the wind shear velocity u^* by the following equation

$$u^* = \sqrt{\frac{\tau}{\rho_a}}$$

where ρ_a is the air density (Kok, 2010). This equation can be rewritten as

$$\tau = \rho_a \, (u^*)^2$$

Saltation occurs when the wind shear velocity u^* is higher than a threshold at which particles on the surface are lifted.

The third parameter, the wind stress lifting rate constant αN, is the constant of proportionality between the vertical flux of dust and the horizontal saltation flux of sand.

The above interactive dust lifting parameters depend on the model resolution. The parameters need to be adjusted by a process known as calibration or tuning. One strategy for tuning is to run the model with different parameters and compare the results to observed data. The parameters which result in data that is closest to the observed data are then improved step-by-step, using trial-and-error.

A model with interactive dust mode is used. Dust is freely lifted, transported, and deposited. The model assumes an uninterrupted and infinite supply of dust particles on the surface. The model in this simulation used the horizontal grid resolution 7.5° x 9°.

2.7 The Beer-Lambert Law

The Beer-Lambert Law (also called Beer's Law) is a relationship between the reduction, or attenuation, of light through a substance and the properties of that substance. Attenuation can be caused by absorption, reflection, scattering and other physical processes.

2.7.1 Derivation of the Lambert Law

Lambert Law states that the decrease in intensity of light as it crosses an absorbing medium is directly proportional to the intensity of the incident light. Mathematically this can be written as:

$$-\frac{dI}{dx} = kI$$

Or

$$-\frac{dI}{I} = kdx$$

Integrating both sides we get

$$\ln I = -kx + C$$

Taking the exponential of both sides, we get

$$I = e^{-kx+C}$$

Using $I = I_0$ when $x = 0$ we get $I = I_0\,e^{-kx}$ or

$$\frac{I}{I_0} = e^{-kx}$$

Again, taking the log of both sides, we get

$$\ln\left(\frac{I}{I_0}\right) = -ax$$

Where a is the extinction coefficient and $A = -\ln\left(\frac{I}{I_0}\right)$ is the absorbance.

2.7.2 The Beer-Lambert Law: Extinction of the Lambert Law

The Beer's Law states that the fraction of incident light absorbed by a solution is proportional to the concentration of the solution. Mathematically:

$$-\frac{dI}{dx} = kc$$

where c is the concentration. Together Lambert's law and Beer's law give

$$-\frac{dI}{dx} = bcI$$

After integrating and rearranging the equation, we get

$$\ln \left(\frac{I}{I_0}\right) = -\varepsilon c x$$

where ε is the molar extinction coefficient.

2.7.3 What are Transmittance and Absorbance?

Consider monochromatic light transmitted through a medium. The transmittance, T, of the medium is defined as the ratio of the transmitted intensity, I, over the incident intensity I_0:

$$T = \frac{I}{I_0} \quad \text{(Notice that } 0 \leq T \leq 1)$$

The absorbance, A, is defined as:

$$A = \ln \left(\frac{I_0}{I}\right) = -\ln(T)$$

This logarithmic relationship shows that when the transmittance T is equal to 1, then A = 0. In other words, there is no absorbance, and the whole incident intensity is transmitted. On the other hand, when T = 0.37 or 37%, then the absorbance A is equal to 1.

The Beer-Lambert law is a linear relationship between the absorbance and the concentration, molar absorption coefficient and optical coefficient of a solution:

$$A = \varepsilon c \ell$$

A	Absorbance	
ε	Molar absorption coefficient	$M^{-1}cm^{-1}$
c	Molar concentration	M
ℓ	Optical path length	cm

The molar absorption coefficient is a sample dependent property and is a measure of how strong an absorber the substance is at a particular wavelength of light. The concentration is simply the number of moles of the sample dissolved per unit volume of the medium, and the optical path length is the length of the medium. In general, the optical depth for any material is

$$A = ln\left(\frac{I_0}{I}\right) = -\ln T$$

2.8 Dust Optical Depth

Measuring the amount of dust present in the Martian atmosphere is particularly challenging at any particular place and time. To overcome this challenge, indirect optical techniques, from orbit or the surface, are used to estimate the opacity of the dust layer Figure 11. This opacity is given at a particular wavelength and can be calculated as an extinction optical depth and is related to the mass mixing ratio of dust M (Forget & Montabone, 2017):

$$\tau = \frac{3M\ Q_{ext}}{4\rho\ r_{eff}}$$

Where;

ρ	*density of the dust material (usually* $2500\ kg\ m^{-3}$*)*
r_{eff}	*effective radius of dust size distribution* $= 2\ \mu m$
Q_{ext}	*single scattering extinction parameter at a given wavelength.*

The column dust optical depth (CDOD) is the extinction optical depth-integrated over the atmospheric column (Forget & Montabone, 2017).
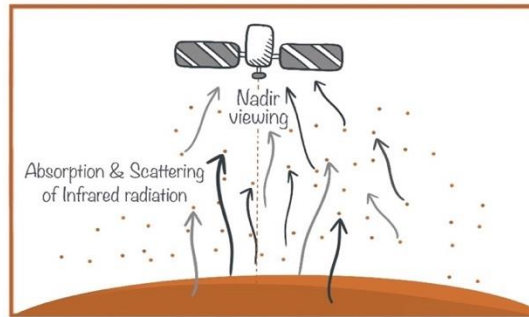
Figure 11: The absorption and scattering of infrared radiation using a satellite with nadir viewing to calculate the column dust optical depth

Dust information can also be retrieved in several ways. These include the use of U.V. wavelength of the solar light, infrared wavelength and from limb viewing satellite instruments.

We also notice how the dust storms are affected by the location relative to the sun. In the dust storm season, dust is enhanced up to the northern midlatitudes. The dust storm season includes southern spring (northern fall) and summer (northern winter) see Figure 12.

Figure 12: The location of Mars with different degrees of solar longitude, showing the dust storm season

2.9 Model Settings

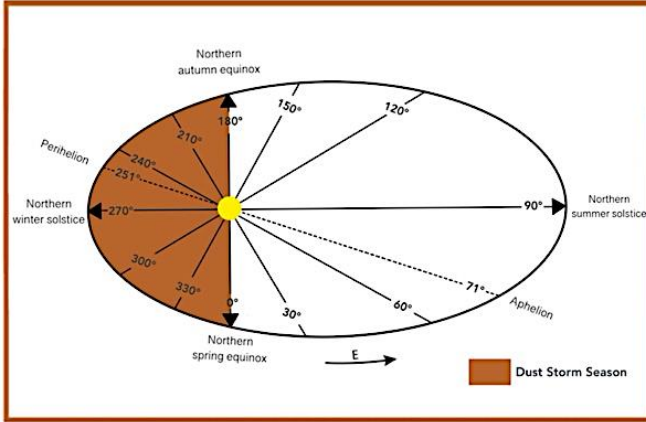The topography is interpolated from the 1/64° Mars Orbiter Laser Altimeter (MOLA) data set (Smith et al., 2001), and MY26 albedo and TES apparent nightside thermal inertia maps are used (Putzig & Mellon, 2007). The model set-up is largely similar to the one used in Gebhardt et al. (2020). One major difference is that the present work uses the resolution of 7.5° × 9°, whereas in Gebhardt et al. (2020), the resolutions are 5° × 5° and 2° × 2°. In the model used in this work:

1. Dust is fully interactive. This means, in particular, that the dust lifting and deposition are produced by the model itself.
2. We assume an infinite supply of dust. As a result, no region runs out of dust.
3. The model generates a surface pressure cycle similar to that recorded by the Viking Landers 1 and 2.
4. A model time step of 1 minute is used, and the output is stored every sol.

5. The study was conducted over 20 Martian years, during the period from Year 1, $L_s = 0°$ and to Year 20, $L_s = 360°$.

2.10 Interactive Dust Mechanism

Three schemes are used in the interactive dust mechanism. The first one is used for gravitational dust sedimentation. The other two are dust lifting mechanisms. The first one is a convective, or dust devil scheme. This scheme represents the dust lifted by hot air vortices that occur during the day as a result of the heating of the Mars surface. The second dust lifting mechanism is a wind stress lifting scheme. This scheme accounts for dust lifted by saltation.

The two dust lifting schemes are controlled by the three parameters. As mentioned earlier in this section, the dust devil lifting rate constant α_D, the wind stress lifting threshold τ, and the wind stress lifting rate constant α_N. These parameters are adjustable by a trial-and-error method.

These parameters are adjusted and tuned to their optimum values by comparing the model results with observed atmospheric properties, such as the T15 temperature curves (Gebhardt et al., 2020). T15 temperature refers to temperatures measured in the 15 μm CO_2 absorption band, which roughly corresponds to an altitude range of 10 to 40 km, with the highest measurement sensitivity at 25 km. The weighted average of the model temperatures over all except the topmost vertical model level is used to calculate the MarsWRF T15 estimates. The average weight of each model level is given by w(p)/p, with w(p) being the vertical weighting function. Average weighting by both w(p) and 1/p ensures an equal representation of all vertical layers. Our model grid has equidistant vertical pressure levels, resulting in the vertical resolution increasing from the model top to bottom in terms of altitude.

Chapter 3

Chapter 3: Results and Discussions

This chapter presents the results of $7.5° \times 9°$ simulations and compares these results with higher resolution of $5° \times 5°$ simulations in Gebhardt et al. (2020). First, based on T15 temperature, we select the best model parameters for $7.5° \times 9°$. We explore other characteristics such as topography and surface dust gain and loss using these parameters.

First, we find the best parameters by repeatedly running the model based on the T15 temperature. As mentioned in Chapter 2, T15 temperature refers to temperatures measured in the 15 μm CO_2 absorption band. For the estimation of global T15 temperatures, model data on T15 are averaged over 40°S to 40°N. We describe and discuss the main findings for the model run with the resolution of $7.5° \times 9°$ and compare them with $5° \times 5°$ resolution simulations in Gebhardt et al. (2020).

3.1 Selection of Parameters and Resulting Dust Storms

The first parameter to be tuned is α_D. Its optimum value was found to be $\alpha_D = 1.6 \times 10^{-9}$. The other two parameters τ and α_N were tuned by trial-and-error using a wide range of possible values. Values of τ equal to 0.04, 0.035 and 0.02 were used in conjunction with values of α_N from 1×10^{-6} and 1.5×10^{-5}. It was found that optimum results were obtained when $\tau = 0.04$ and $\alpha_N = 1.4 \times 10^{-5}$ (Table 1).

Table 1: The trial numbers with different values of the two parameters τ and α_N tuned by trial-and-error

Trail Number	τ (Pa)	α_N
1	0.02	1×10^{-6}
2	0.02	1.8×10^{-6}
3	0.02	2×10^{-6}
4	0.035	1.7×10^{-6}
5	0.035	1×10^{-5}
6	0.04	1.5×10^{-6}
7	0.04	1.8×10^{-6}
8	0.04	1×10^{-5}
9	0.04	1.5×10^{-5}
10	0.04	1.4×10^{-5}

The results are shown in Figure 13 for 20 MYs. They are consistent with knowledge from observations that, on average, every ten years, there are 3-4 global dust storms. Figure 13a shows the T15 temperature for MY Year 1 to Year 10. The T15 temperature refers to temperatures measured in the 15 μm CO_2 absorption band, representing roughly the altitude range from 10 to 40 km, with the maximum measurement sensitivity at ca. 25 km. There are three Martian years with GDEs, Year 1, Year 4, and Year 5. The second T15 temperature plot, Figure 13b, is for Year 11 to Year 20. Clearly, Years 11 and 12 are showing a Global Dust Storm event. Dust storm events raise the planet's temperature. This high temperature shows as a peak during the dust storm season ($L_s = 250° - 360°$). The black dashed line is the climatological background based on observations. The curves show specific

years with steep temperature increases starting at $L_s = 250°$ and peaking at around $L_s = 300°$ to represent the global dust storm events.
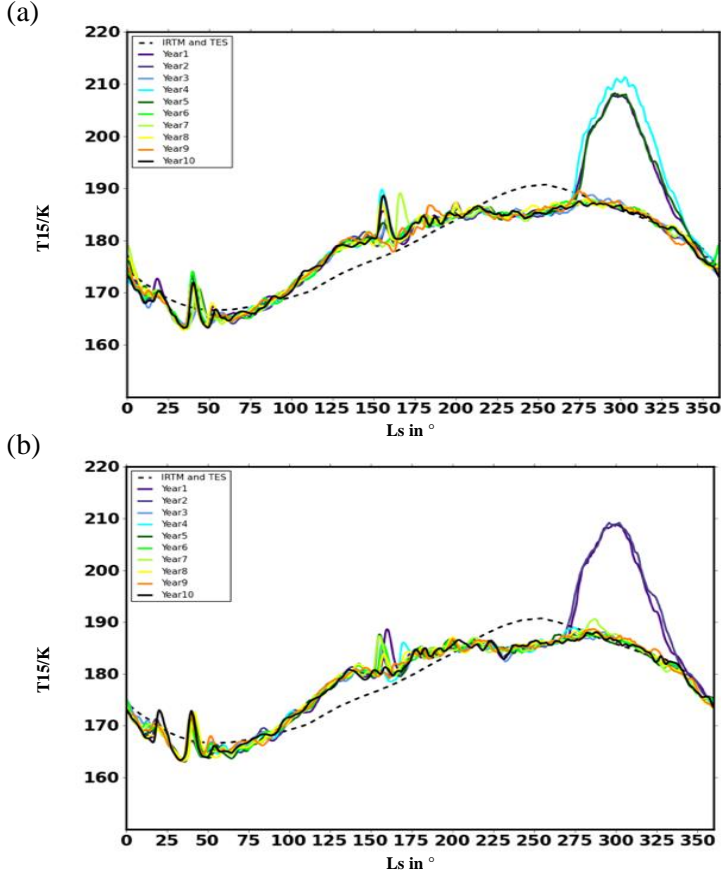
(a)

(b)

Figure 13: Two plots of the T15 temperature (a) MarsWRF simulated global T15 temperature curves for the $7.5° \times 9°$ model run, from year 1 to 10, (b) is the same, but for the next 10 MY (year 11 to year 20), $\tau = 0.02$ and $\alpha_N = 1.4 \times 10^{-5}$ $\alpha_D = 1.6 \times 10^{-9}$

In comparing the 7.5° × 9° (Figure 13a) and the 5° × 5° (Figure 14), we notice that there is a slight difference in the T15 temperature. In 7.5° × 9° resolution, along with GDEs and non-major dust storm events, T15 temperatures above 200 K have been noticed in Year 1. This is not the case for the resolution 5° × 5° model. Year 3 appears as GDE in the resolution 5° × 5° but not in the resolution 7.5° × 9°. Year 4 and Year 5 appear in both resolutions.

This difference between the two models depends on the interaction of major dust lifting regions at low latitudes. In fact, GDEs develop if regional dust storm activity south of Chryse Planitia and northeast of Valles Marineris connects with that on the northern slopes of the Hellas basin. Without this connection, the peak T15 never exceeds 200 K.

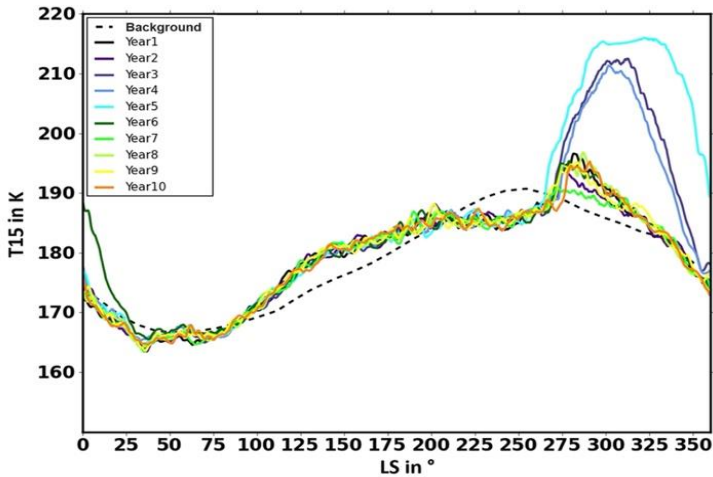Figure 14: T15 temperature for 5° × 5° resolution

For values of the parameters that correspond to non-optimal simulations, the plots will either display a repetitive pattern or just randomly display high peaks as shown Figure 15. This means the model failed to predict T15 peaks in few MY only.
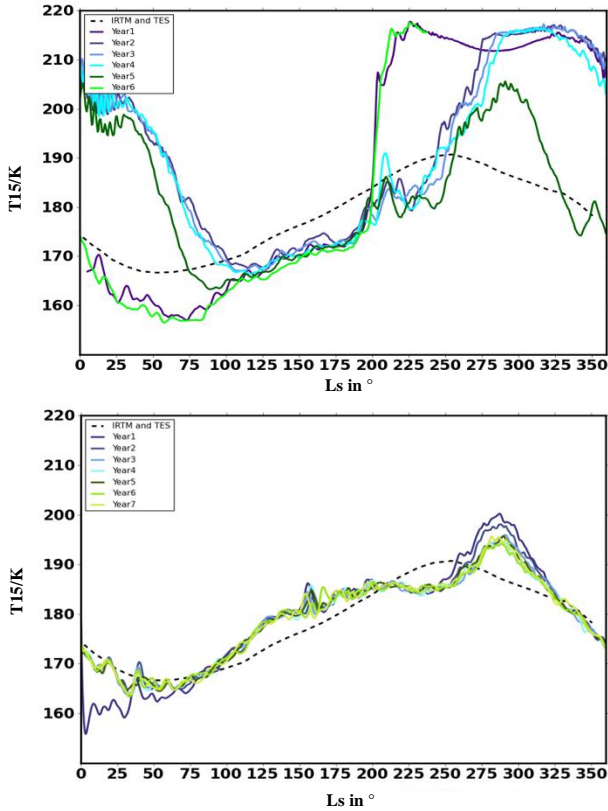

Figure 15: Two plots of T15 temperature, where the parameters were not optimal and the results are not clear

3.2 Model Topography

This thesis is based on using the MarsWRF model. The model captured important surface features, such as the Hellas basin, Valles Marineris, Olympus Mons, the Tharsis volcanoes, Elysium Mons, and their associated topographic slopes. First, we present the topography results of the resolution of $7.5° \times 9°$. As explained earlier, topography has a significant impact on dust storms. The MarsWRF model was built up in a $7.5° \times 9°$ resolution with the model topography shown in Figure 16a. Surface features and their associated topographic slopes are showing, especially in regions like Hellas basin (HB), Alba Mons (AM), Olympus Mons (OM), Tharsis Montes (TM) and Tharsis Rise (TR).

The $7.5° \times 9°$ topography shows fewer details than the higher resolution of $5° \times 5°$ in Figure 16b. The two models show roughly the same topography, but there are more details in the $5° \times 5°$ resolution. The contours are more intricate. In addition, high or low altitudes such as Elysium Mons (EM), Argyre Basin (AB) and Valles Marineris (VM) show more clearly in the higher resolution.
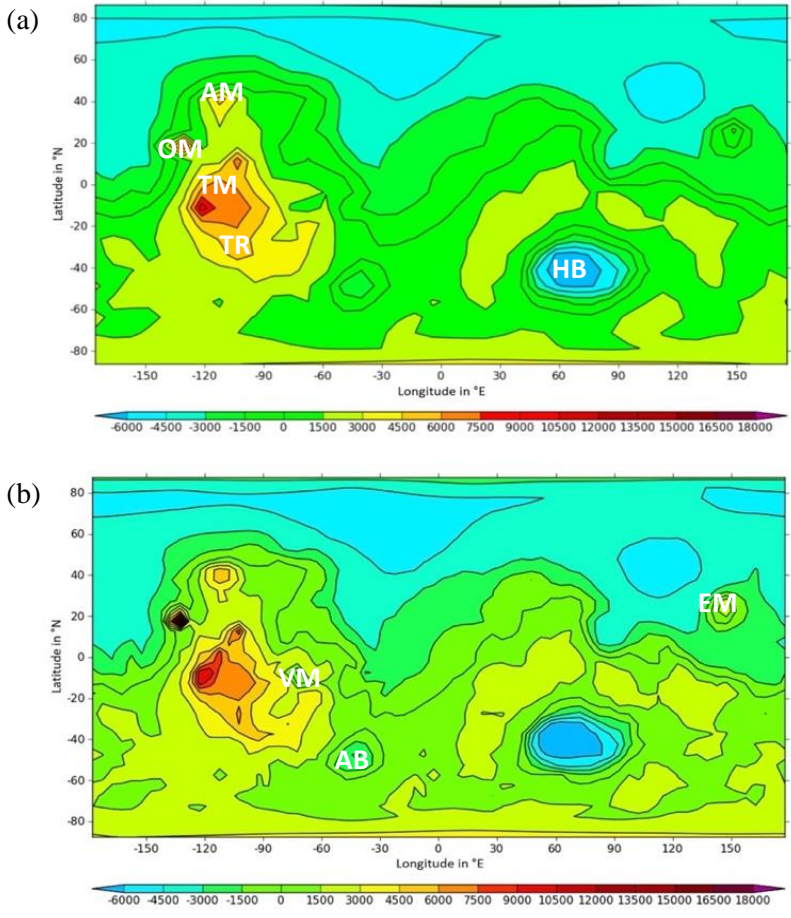
Figure 16: Two plots of the model topography for different resolution (a) Model topography for the resolution $7.5° \times 9°$, (b) Model topography for the resolution $5° \times 5°$

3.3 Dust Optical Depth

Figure 17 shows dust optical depth for the resolution $7.5° \times 9°$, which is a measure of the extinction of solar radiation by dust. Dust particles are radiatively active. They absorb solar radiation and emit and absorb infrared radiation from the sun. Therefore, they affect atmospheric temperature when they heat up or cool down. The plots show two different sols in Year 4. Figure 17a Indicates surface dust lifting around the area of Olympus Mons (OM), Alba Mons (AB), Tempe Terra (TT) and near Arabia Terra (AT). Figure 17b shows the dust optical depth generated in Hellas Basin (HB) and Hesperia Planum (HP).
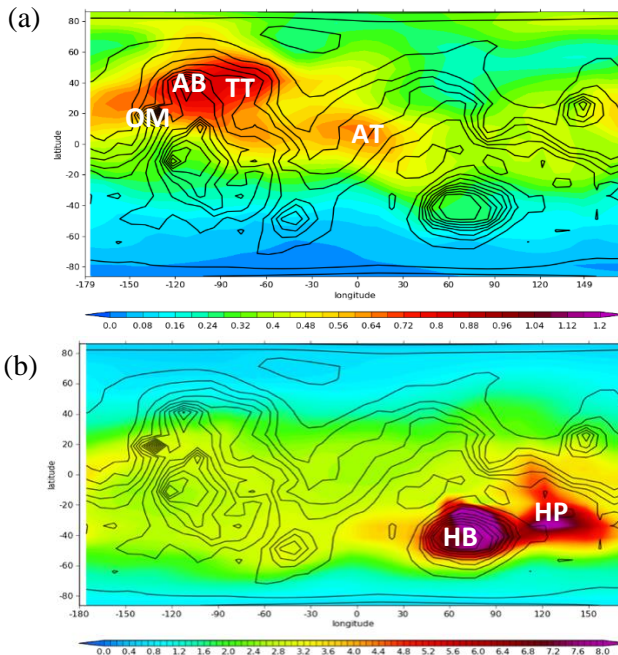

Figure 17: Plots of dust optical depth for the resolution $7.5° \times 9°$. (a) Showing the dust loss around the Olympus Mons (OM), Alba Mons (AB), Tempe Terra (TT) and near Arabia Terra (AT) (b) Dust optical depth in Hellas Basin (HB) and Hesperia Planum (HP)

3.3.1 Dust Optical Depth and Solar longitude

There are specific seasons for dust on Mars. There is seasonal variation in aerosol optical depth that is dependent on the solar longitude. Figure 18 shows the dust optical depth for eight different solar longitudes in Year 4 for the resolution $7.5° \times 9°$, a year that contained no GDEs. While Figure 19 shows a Martian year with GDEs Year 6 for the resolution $7.5° \times 9°$. The generation of the dust storm in Figure 19 can be seen in the solar longitude of 270. It is clear that the dust is more active in Year 6 than in Year 4, especially at the $L_s = 315°$, which is during the dust storm season. The dust covers most areas between the Latitudes -70 and 30.

Figure 18: Column dust optical depth for different solar longitude in Year 4 for the resolution 7.5° × 9°. (a) $L_s = 45°$ (b) $L_s = 90°$ (c) $L_s = 135°$ (d) $L_s = 180°$ (e) $L_s = 225°$ (f) $L_s = 270°$ (g) $L_s = 315°$ (h) $L_s = 360°$

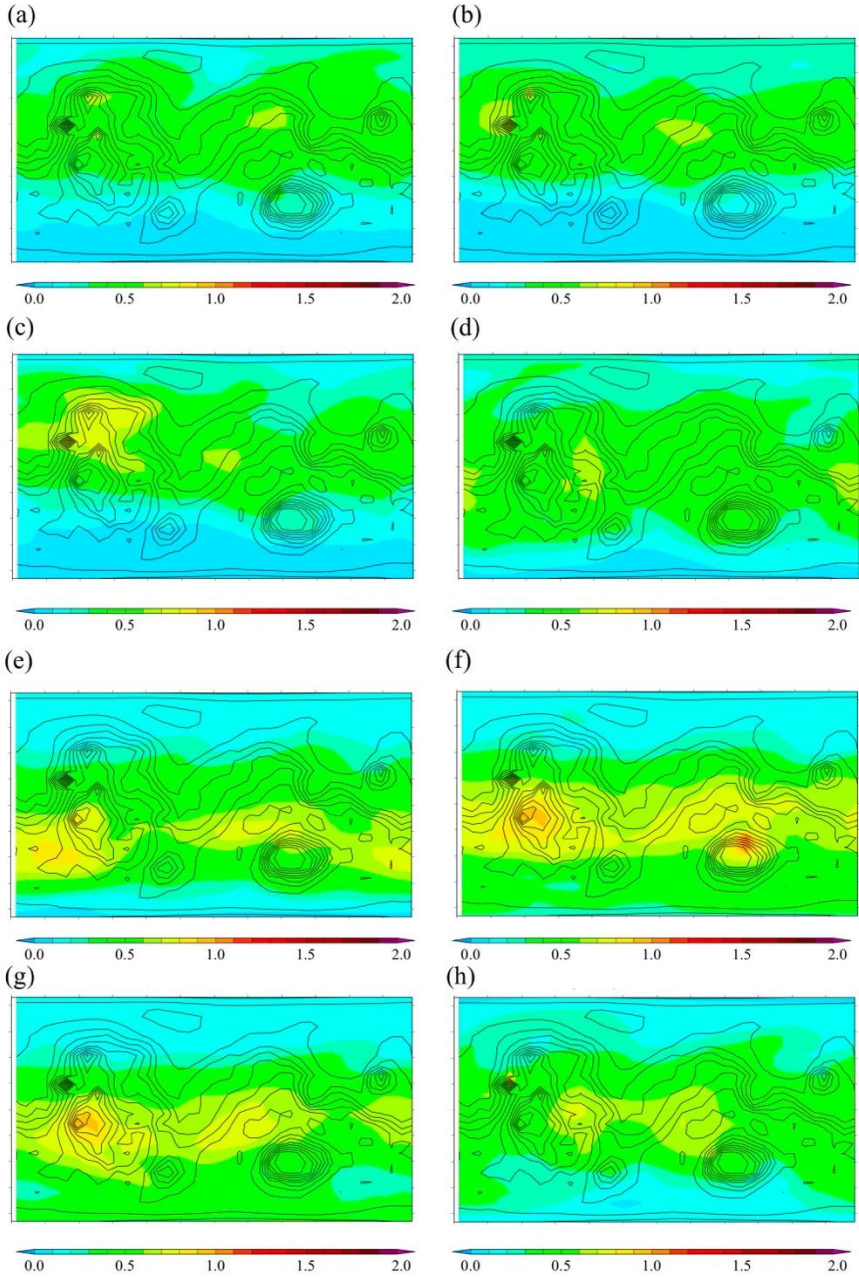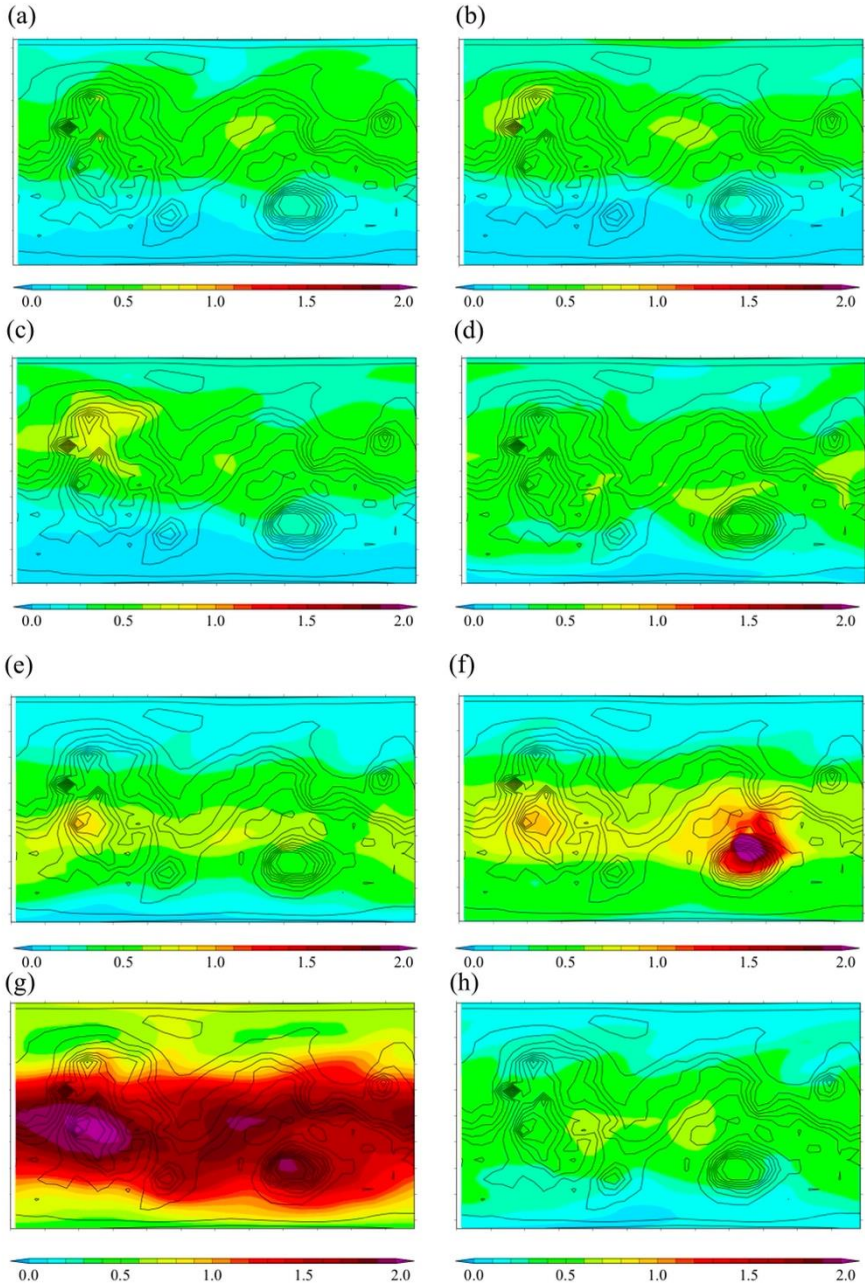Figure 19: Column dust optical depth for different solar longitude in Year 6 for the resolution $7.5° \times 9°$. (a) $L_s = 45°$ (b) $L_s = 90°$ (c) $L_s = 135°$ (d) $L_s = 180°$ (e) $L_s = 225°$ (f) $L_s = 270°$ (g) $L_s = 315°$ (h) $L_s = 360°$

3.4 Dust Devils

Dust lifting is the sum of all dust lifted per area during ten Sols. Figure 20a shows the dust devil lifting (kg m^{-2} per 10 Sols) for the $7.5° \times 9°$ model run from Year 1 sol 1 to Year 10 sol 669. The $7.5° \times 9°$ model run has some similarities with the simulations done by Gebhardt et al. (2020). In Figure 20b, a resolution of $5° \times 5°$ is used.

According to the $7.5° \times 9°$ model run, the area that has the highest probabilities of dust devil activity are Amazonis Planitia (AP), Olympus Mons (OM), Alba Mons (AM), Tempe Terra (TT), Tharsis Montes (TM), northern Elysium Mons (N-EM) and the northern Hellas Basin (N-HB). The spatial distribution of dust devils follows areas that have higher altitudes. It was found that dust lifting by the dust devil scheme occurs mostly along with the latitude bands of $\simeq 20$–$40°$N/S. It was also observed that dust devils occur around some Martian volcanoes such as Olympus Mons (OM), Alba Mons (AM), Tharsis Montes (TM) and northern Elysium Mons (N-EM).

Although the $5° \times 5°$ is more detailed and employs finer resolution simulations, the results are similar for both resolutions and imply that resolution is not a major factor in dust devils' occurrence and spatial distribution.
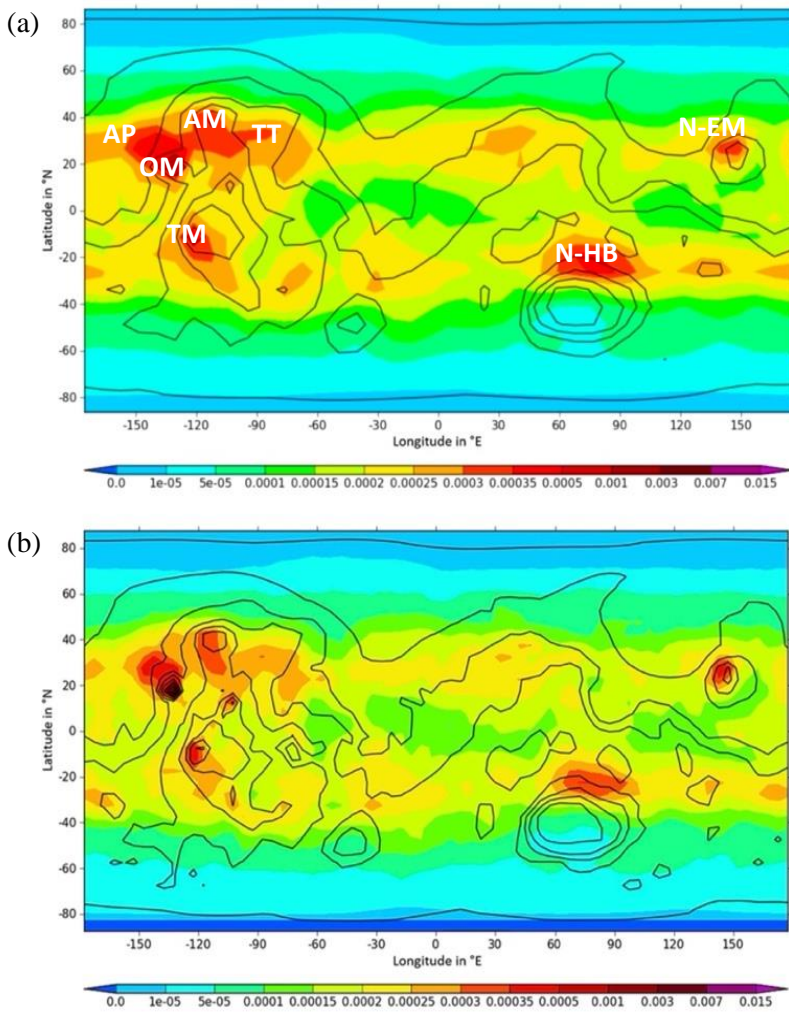
Figure 20: Dust devil lifting (mass per unit area per 10 sols) (a) For the resolution 7.5° × 9°, (b) Dust devil lifting for the resolution of 5° × 5°

3.5 Wind Stress

Figure 21a shows the average of the surface dust lifting by wind stress (kg m^{-2} per 10 Sols) from Year 1 to Year 10. Studying wind stress is important to understand the movement of dust on the Mars surface and atmosphere and, therefore, the places of dust loss and dust gain. For the resolution 7.5° × 9° the main regions losing dust are northern Olympus Mons (N-OM), Alba Mons (AM) and the northern Hellas Basin plain (N-HB). There is also some dust lifting in western Olympus Mons (W-OM) and Isidis Basin (IB). Figure 21b for the 5° × 5° resolution has more details in explaining the wind stress in comparison to the 7.5° × 9° resolution (Figure 21a). It covers more areas than the 7.5° × 9° resolution, such as Tempe Terra (TT), southern and eastern Tharsis Rise (S-TR, E-TR), Utopia Basin (UB), northern Elysium Mons (EM). The resolution of 5° × 5° also shows wider areas in the northern Hellas Basin (N-HB) and Alba Mons (AB).

According to the plots, the main wind stress lifting regions are well defined in the 5° × 5° resolution model run. In this higher resolution, wind stress lifting occurs across the whole planet, covering many areas. The two simulations exhibit a contrast in the findings of wind stress lifting regions. This contrast is due to the differences in the wind stress lifting model parameters along with atmospheric circulation and model topography.
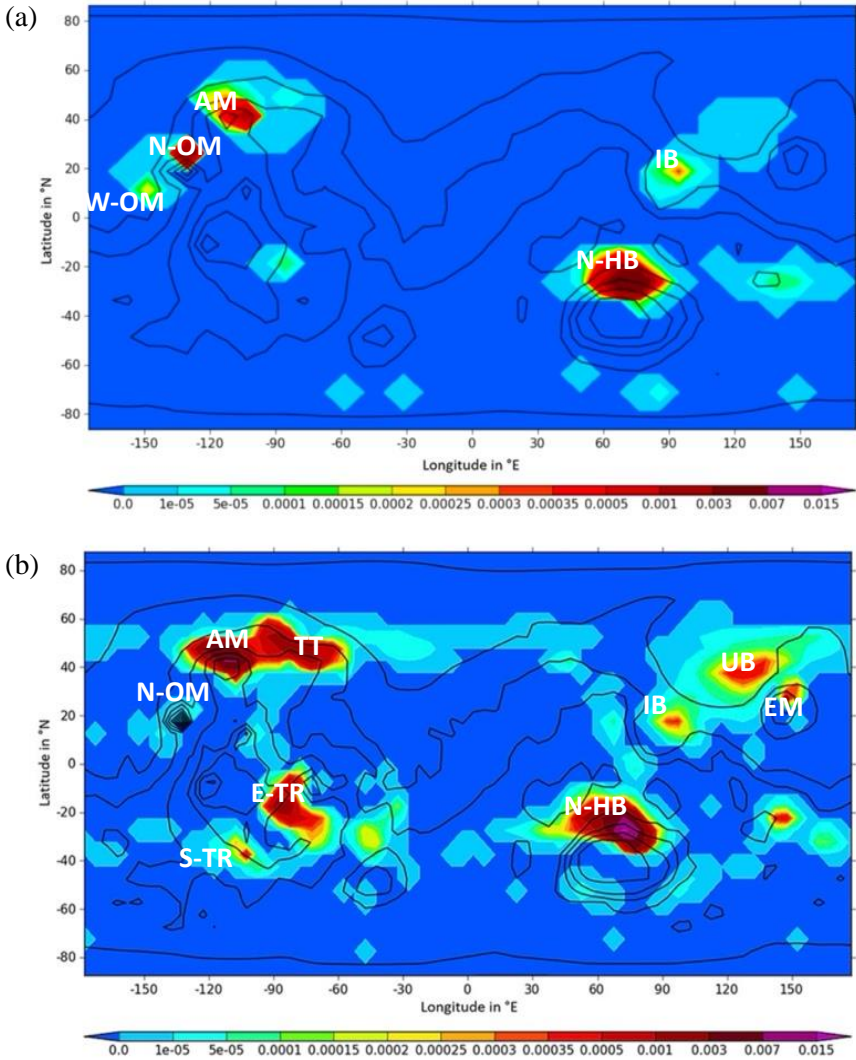
Figure 21: Average of the surface dust lifting by wind stress (a) For the resolution of 7.5° × 9°, (b) For the resolution of 5° × 5°

Furthermore, it was observed that the time-average near-surface wind patterns on a large scale are not particularly sensitive to resolution. The vast majority of changes in surface wind stress patterns with increased

resolution can be considered as the linear superposition of large-scale wind patterns and local scale circulations due to topography (e.g., craters, volcanoes, canyons, etc.).

According to Figure 22, topography has a huge impact on dust lifting by wind stress. The grid points show the wind stress lifting. There are specific regions on Mars that contribute more dust than others. These include high volcanoes like Olympus Mons and Alba Mons or deep plains like Hellas Basin. Figure 22b, for the resolution $5° \times 5°$ model run, shows grid points covering almost the whole map. Areas between latitudes 40-60 appear to have high areas of dust loss. Both plots show strong surface dust lifting areas in the western Olympus Mons, Alba Mons, southern Tharsis Rise, Isidis Basin, Utopia Basin, northern Hellas Basin and Hesperia Planum. The red and yellow grids refer to large dust loss in these regions, as in northern Hellas Basin and Alba Mons.
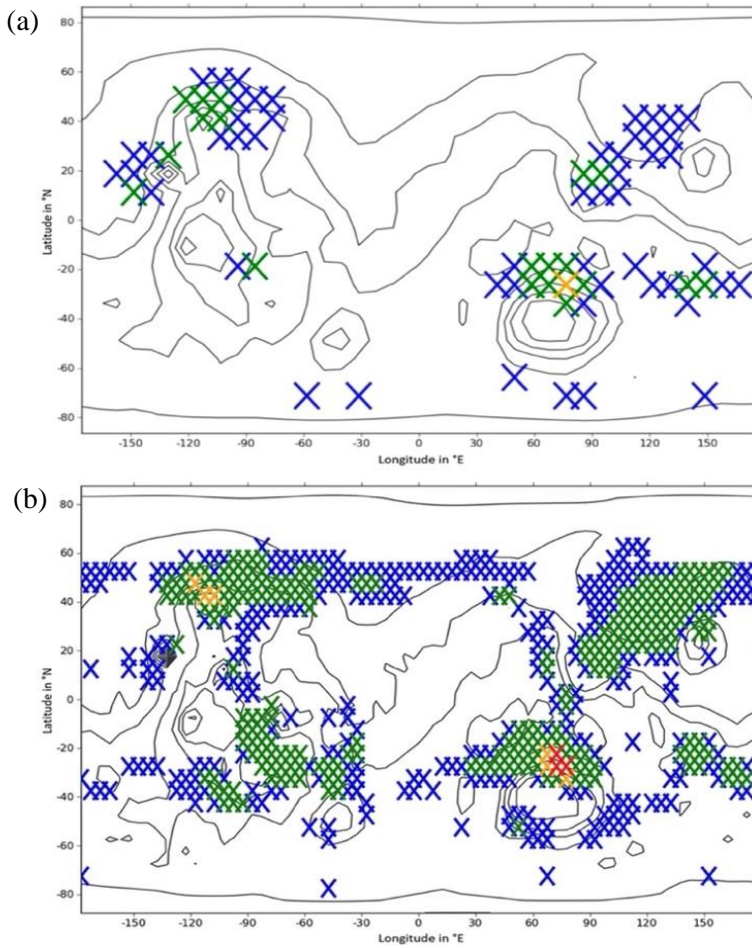
Figure 22: Surface dust lifting by wind stress (a) Grid points of the 7.5° × 9° model run. (b) Grid points of the 5° × 5° model run

3.6 Change in Surface Dust Cover

In general, change in surface dust cover refers to the areas where dust is freely available to uplift and areas where dust is deposited. Change in surface dust is the result of dust lifting by wind stress and dust devils, and dust deposition. Since we assume an infinite dust supply, dust cover for all areas is potentially subject to change. The analysis here is from the first sol in Year 1 to the last sol in Year 10 (kg m^{-2}).

Figure 23: Change in surface dust cover (units of kg m^{-2}) (a) for the resolution 7.5° × 9° (b) for the resolution of 5° × 5°

Figure 23a shows the change in a surface dust cover for the resolution of 7.5° × 9°. The pronounced dust gain regions are located in all latitudes, from low to middle, to high latitudes, as indicated in the figure by purple and red. The green areas are those where dust is uplifted into the atmosphere; therefore, dust losing areas. Hellas Basin net surface dust cover change seems to be negat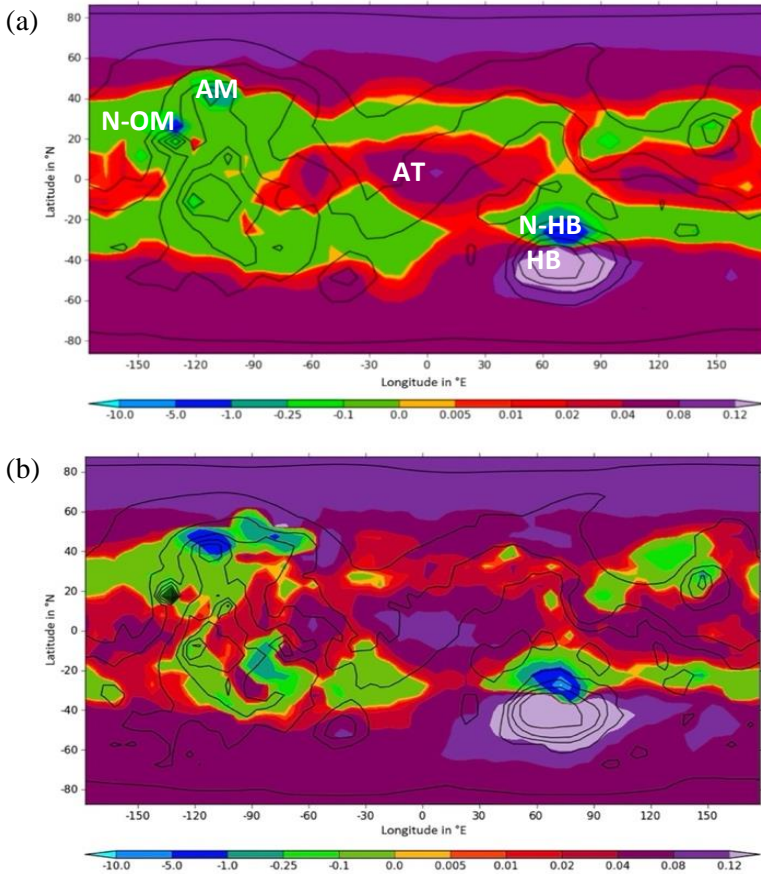ive. This is due to that fact that although the blue region is small compared to the purple one, its value is negative and 100 times larger than the purple one. Other areas such as Arabia Terra also show some dust gain. The northern Hellas Basin (N-HB), northern Olympus Mons (N-OM) and Alba Mons (AM) present the highest dust loss.

This is similar to the simulation of 5° × 5° that is shown in Figure 23b. In the simulation of a high-resolution experiment, it was found that Global Dust Events on Mars take place with regional dust storm activity. It was noticed that the change in dust activity in two equatorial source regions on the planet that are south of Chryse Planitia and in the Hellas basin triggered Global Dust Events on Mars.

East of Alba Mons shows a dust gain at 7.5° × 9°, while at 5° × 5°, there is substantial dust loss. Olympus Mons and southeast of Tharsis also appear to be different in the two resolutions. There is dust gain in these regions for 5° × 5°, while there is dust loss for the resolution of 7.5° × 9°.

The two figures show that regions of latitudes greater than 60 experience high dust gain. Figure 23a shows that large areas, between the Latitude -40 and Latitude 40 experience dust loss, with a few regions seeing a dust gain. On the other hand, the higher resolution Figure 23b shows that between the Latitudes -40 and 40, the area with dust loss is actually smaller, and the area where there was a dust gain is much larger than those for the resolution of 7.5° × 9° in Figure 23a.

Here in Figure 24, we compare the result of the dust cover of 7.5° × 9° with Figure 14 of Ruff & Christensen (2002). According to the Dust Cover Index (DCI) map, there is a certain degree of similarity in areas between latitudes -40 to 60. Regions like Arabia Terra and Hesperia Planum present dust gain in both figures. Areas like Amazonis Planitia, Olympus Mons, Tharsis Montes, Utopia Basin and Elysium Mons present a dust loss in the 7.5° × 9° model run and the Ruff and Christensen model.
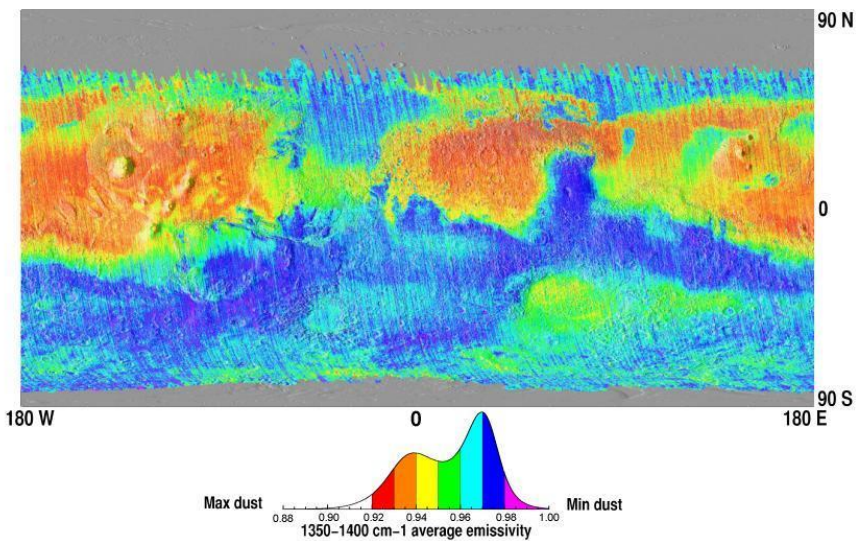

Figure 24: Global Dust Cover of the DCI from Ruff & Christensen (2002)

Chapter 4

Chapter 4: Conclusion

This thesis is based on the MarsWRF models for the resolution of 7.5°×9° and the higher resolution of 5°×5° in Gebhardt et al. (2020) and their intercomparison. The models and simulations include Interactive dust at 7.5°×9° horizontal resolution. The study examines the impact of the 7.5°×9° resolution on the Martian global atmosphere and climate simulation.

To start with, the study identified major dust lifting regions north of the Hellas Basin and the north of Olympus Mons. The comparison is carried out both on a regional and global base. The result shows more surface wind stress and dust lifting in the 5°×5° model run than in simulation 7.5°×9° at both regional and global levels. Such variation is due to the presence or absence of radiative dust dynamics on a regional and global scale.

When we assume the same for other regions of Hellas Basin and North of Olympus Mons, the excess factors in surface dust lifting provide an upper estimate or constraint on the increase of dust storm strength and duration. The dynamics of Mars dust storms include certain features which deserve special attention. The patterns of surface dust change for simulations exhibit strong dust gain inside the Hellas Basin, with a high degree of similarity. Moreover, the nearby dust lifting region is of similar strength in both models. This is governed by great differences in the topography representation of some regions like Tharsis Montes, Alba Mons and Elysium Mons.

The results indicate that the 5°×5° and 7.5°×9° models are similar to each other, with certain differences around some regions. However, the 5°×5° shows more details in some areas, but in the 7.5°×9°, there were interesting significant results that are not in the 5°×5° model run. Using the

classical resolution of 7.5°×9° was a good choice for a master thesis since the simulation done with higher resolutions will require more computational time.

For future work, one can continue forecasting Mars global dust storms by running the model with finite dust for different resolutions. The finite dust model gives more realistic results, which help to get better forecasting for dust storm events on Mars. But there is a cost. Using higher resolution requires more time, but it will help with getting more details.

References

Basu, S., Richardson, M. I., & Wilson, R. J. (2004). Simulation of the Martian dust cycle with the GFDL Mars GCM. *Journal of Geophysical Research: Planets*, *109*(11), 1–25. https://doi.org/10.1029/2004JE002243

Basu, S., Wilson, J., Richardson, M., & Ingersoll, A. (2006). Simulation of spontaneous and variable global dust storms with the GFDL Mars GCM. *Journal of Geophysical Research*, *111*(E9), E09004. https://doi.org/10.1029/2005JE002660

Battalio, M., & Wang, H. (2019). The Aonia-Solis-Valles dust storm track in the southern hemisphere of Mars. *Icarus*, *321*, 367–378. https://doi.org/10.1016/j.icarus.2018.10.026

Battalio, M., & Wang, H. (2021). The Mars Dust Activity Database (MDAD): A comprehensive statistical study of dust storm sequences. *Icarus*, *354*, 114059. https://doi.org/10.1016/j.icarus.2020.114059

Bertrand, T., Wilson, R. J., Kahre, M. A., Urata, R., & Kling, A. (2020). Simulation of the 2018 Global Dust Storm on Mars Using the NASA Ames Mars GCM: A Multitracer Approach. *Journal of Geophysical Research: Planets*, *125*(7), 361–374. https://doi.org/10.1029/2019JE006122

Bridges, N. T., Bourke, M. C., Geissler, P. E., Banks, M. E., Colon, C., Diniega, S., Golombek, M. P., Hansen, C. J., Mattson, S., McEwen, A. S., Mellon, M. T., Stantzos, N., & Thomson, B. J. (2012). Planet-wide sand motion on Mars. *Geology*, *40*(1), 31–34. https://doi.org/10.1130/G32373.1

Cantor, B. A., James, P. B., Caplinger, M., & Wolff, M. J. (2001). Martian dust storms: 1999 Mars Orbiter Camera observations. *Journal of Geophysical Research: Planets*, *106*(E10), 23653–23687. https://doi.org/10.1029/2000JE001310

European Space Agency Publications (2022) https://www.esa.int/ESA_Multimedia/Images/2021/02/Mars_dust_devils_in_action

Forget, F., Hourdin, F., Fournier, R., Hourdin, C., Talagrand, O., Collins, M., Lewis, S. R., Read, P. L., & Huot, J. P. (1999). Improved general circulation models of the Martian atmosphere from the surface to above 80 km. *Journal of Geophysical Research: Planets*, *104*(E10), 24155–24175. https://doi.org/10.1029/1999JE001025

Forget, F., & Montabone, L. (2017). Atmospheric Dust on Mars: A Review. 47th International Conference on Environmental Systems (ICES), 16-20 July 2017.

Gebhardt, C., Abuelgasim, A., Fonseca, R. M., Martín-Torres, J., & Zorzano, M. P. (2020). Fully Interactive and Refined Resolution Simulations of the Martian Dust Cycle by the MarsWRF Model. *Journal of Geophysical Research: Planets*, *125*(9), 213-233. https://doi.org/10.1029/2019JE006253

Guzewich, S. D., Toigo, A. D., Richardson, M. I., Newman, C. E., Talaat, E. R., Waugh, D. W., & McConnochie, T. H. (2013). The impact of a realistic vertical dust distribution on the simulation of the Martian General Circulation. *Journal of Geophysical Research: Planets*, *118*(5), 980–993. https://doi.org/10.1002/jgre.20084

Haberle, R. M., Kahre, M. A., Murphy, J. R., Christensen, P. R., & Greeley, R. (2006). Role of dust devils and orbital precession in closing the Martian dust cycle. *Geophysical Research Letters*, *33*(19), L19S04. https://doi.org/10.1029/2006GL026188

Heavens, N. G., Cantor, B. A., Hayne, P. O., Kass, D. M., Kleinböhl, A., McCleese, D. J., Piqueux, S., Schofield, J. T., & Shirley, J. H. (2015). Extreme detached dust layers near Martian volcanoes: Evidence for dust transport by mesoscale circulations forced by high topography. *Geophysical Research Letters*, *42*(10), 3730–3738. https://doi.org/10.1002/2015GL064004

Ho C., Golshan N., and Kliore, A. (2002). *Radio Wave Propagation Handbook for Communication on and Around Mars.* NASA JPL-Publication 02-5, pp. 59-71.

Jakosky, B. M., Mellon, M. T., Kieffer, H. H., Christensen, P. R., Varnes, E. S., & Lee, S. W. (2000). The thermal inertia of Mars from the Mars Global Surveyor Thermal Emission Spectrometer. *Journal of Geophysical Research: Planets*, *105*(E4), 9643–9652. https://doi.org/10.1029/1999JE001088

Kahre, M. A., Murphy, J. R., & Haberle, R. M. (2006). Modeling the Martian dust cycle and surface dust reservoirs with the NASA Ames general circulation model. *Journal of Geophysical Research*, *111*(E6), E06008. https://doi.org/10.1029/2005JE002588

Kahre, M. A., Murphy, J. R., Newman, C. E., Wilson, R. J., Cantor, B. A., Lemmon, M. T., & Wolff, M. J. (2017). The Mars Dust Cycle. In *The Atmosphere and Climate of Mars* (pp. 295–337). Cambridge University Press. https://doi.org/10.1017/9781139060172.010

Kok, J. F. (2010). *Analytical calculation of the minimum wind speed required to sustain wind-blown sand on Earth and Mars*. arXiv preprint. https://doi.org/10.48550/arXiv.1001.4840.

Laux, P., Phan, V. T., Lorenz, C., Thuc, T., Ribbe, L., & Kunstmann, H. (2013). *Setting up regional climate simulations for Southeast Asia*. In W. Nagel, D. Kröner, & M. Resch (Eds.), High Performance Computing in Science and Engineering '12. Berlin/Heidelberg, Germany: Springer.

Lee, C., Richardson, M. I., Newman, C. E., & Mischna, M. A. (2018). The sensitivity of solsticial pauses to atmospheric ice and dust in the MarsWRF General Circulation Model. *Icarus*, *311*, 23–34. https://doi.org/10.1016/j.icarus.2018.03.019

Leovy, C., & Mintz, Y. (1969). Numerical Simulation of the Atmospheric Circulation and Climate of Mars. *Journal of the Atmospheric Sciences*, *26*(6), 1167–1190. https://doi.org/10.1175/1520-0469(1969)026<1167:NSOTAC>2.0.CO;2

Levine, J. S., Kraemer, D. R., & Kuhn, W. R. (1977). Solar radiation incident on Mars and the outer planets: Latitudinal, seasonal, and atmospheric effects. *Icarus*, 31(1), 136–145. https://doi.org/10.1016/0019-1035(77)90076-8

Liu, J. (2003). An assessment of the global, seasonal, and interannual spacecraft record of Martian climate in the thermal infrared. *Journal of Geophysical Research*, *108*(E8), 5089. https://doi.org/10.1029/2002JE001921

Montabone, L., & Forget, F. (2018). *On forecasting dust storms on Mars.* Paper presented at the 48th international conference on environmental systems, Albuquerque. NM, USA, 8–12 July 2018.

NASA (2007).
https://www.nasa.gov/centers/goddard/news/topstory/2007/mars_v
olcanoes.html

NASA Publications (2000a).
https://descanso.jpl.nasa.gov/propagation/mars/MarsPub_sec5.pdf

NASA Publications (2000b). *Planetary laser altimetry*.
https://tharsis.gsfc.nasa.gov/

NASA Publications (2022). https://www.nasa.gov/content/carbon-dioxide-
cycle

NASA Publications (2018).
https://photojournal.jpl.nasa.gov/catalog/PIA02985

Newman, C., Bertrand, T., Battalio, J., Day, M., Juárez, M. D. L. T., Elrod,
M. K., Esposito, F., Fenton, L., Gebhardt, C., Greybush, S. J.,
Guzewich, S. D., Kahanpää, H., Kahre, M., Karatekin, Ö.,
Jackson, B., Lapotre, M., Lee, C., Lewis, S. R., Lorenz, R. D., …
Zorzano, M.-P. (2021). Toward More Realistic Simulation and
Prediction of Dust Storms on Mars. *Bulletin of the AAS*, *53*(4),
14623-14629. https://doi.org/10.3847/25c2cfeb.726b0b65

Newman, C. E., Lee, C., Mischna, M. A., Richardson, M. I., & Shirley, J.
H. (2019). An initial assessment of the impact of postulated orbit-
spin coupling on Mars dust storm variability in fully interactive
dust simulations. *Icarus*, *317*, 649–668.
https://doi.org/10.1016/j.icarus.2018.07.023

Newman, C. E., Lewis, S.R., Read, P.L., & Forget, F. (2002). Modeling
the Martian dust cycle, 1. Representations of dust transport
processes. *Journal of Geophysics Research: Planets, 107*(E12),
5123.
https://10.1029/2002JE001920

Newman, C. E., Lewis, S. R., Read, P. L., & Forget, F. (2002). Modeling
the Martian dust cycle 2. Multiannual radiatively active dust
transport simulations. *Journal of Geophysical Research: Planets,
107*(E12), 5124. https://doi.org/10.1029/2002je001920

Newman, C. E., & Richardson, M. I. (2015). The impact of surface dust
source exhaustion on the martian dust cycle, dust storms and
interannual variability, as simulated by the MarsWRF General
Circulation Model. *Icarus*, *257*, 47–87.
https://doi.org/10.1016/j.icarus.2015.03.030

Petrosyan, A., Galperin, B., Larsen, S. E., Lewis, S. R., Määttänen, A., Read, P. L., Renno, N., Rogberg, L. P. H. T., Savijärvi, H., Siili, T., Spiga, A., Toigo, A., & Vázquez, L. (2011). the Martian atmospheric boundary layer. *Reviews of Geophysics*, *49*(3), RG3005. https://doi.org/10.1029/2010RG000351

Putzig, N., & Mellon, M. (2007). Apparent thermal inertia and the surface heterogeneity of Mars. *Icarus*, *191*(1), 68–94. https://doi.org/10.1016/j.icarus.2007.05.013

Raack, J., Reiss, D., Balme, M. R., Taj-Eddine, K., & Ori, G. G. (2018). In Situ Sampling of Relative Dust Devil Particle Loads and Their Vertical Grain Size Distributions. *Astrobiology*, *18*(10), 1305–1317. https://doi.org/10.1089/ast.2016.1544

Renno, N. O. & Ingersoll, A. P. (1996). Natural convection as a heat engine: A theory for CAPE. *Journal of Atmospheric Sciences, 53*(4), 572-585. https://doi.org/10.1175/1520-0469(1996)053<0572:NCAAHE>2.0.CO;2.

Rennó, N. O., Burkett, M. L., & Larkin, M. P. (1998). A Simple Thermodynamical Theory for Dust Devils. *Journal of the Atmospheric Sciences*, *55*(21), 3244–3252. https://doi.org/10.1175/1520-0469(1998)055<3244:ASTTFD>2.0.CO;2

Richardson, M. I., Toigo, A. D., & Newman, C. E. (2007). PlanetWRF: A general purpose, local to global numerical model for planetary atmospheric and climate dynamics. *Journal of Geophysical Research: Planets*, *112*(9). https://doi.org/10.1029/2006JE002825

Ruff, S. W., & Christensen, P. R. (2002). Bright and dark regions on Mars: Particle size and mineralogical characteristics based on Thermal Emission Spectrometer data. *Journal of Geophysical Research: Planets*, *107*(E12), 5119-5131. https://doi.org/10.1029/2001JE001580

Smith, D. E., Zuber, M. T., Frey, H. V., Garvin, J. B., Head, J. W., Muhleman, D. O., Pettengill, G. H., Phillips, R. J., Solomon, S. C., Zwally, H. J., Banerdt, W. B., Duxbury, T. C., Golombek, M. P., Lemoine, F. G., Neumann, G. A., Rowlands, D. D., Aharonson, O., Ford, P. G., Ivanov, A. B., … Sun, X. (2001). Mars Orbiter Laser Altimeter: Experiment summary after the first year of global mapping of Mars. *Journal of Geophysical Research: Planets*, *106*(E10), 23689–23722. https://doi.org/10.1029/2000JE001364

Toigo, A. D., Lee, C., Newman, C. E., & Richardson, M. I. (2012). The impact of resolution on the dynamics of the martian global atmosphere: Varying resolution studies with the MarsWRF GCM. *Icarus*, *221*(1), 276–288. https://doi.org/10.1016/j.icarus.2012.07.020

Toigo, A. D., Waugh, D. W., & Guzewich, S. D. (2020). Atmospheric transport into polar regions on Mars in different orbital epochs. *Icarus*, *347*, 113816. https://doi.org/10.1016/j.icarus.2020.113816

Wang, H., & Richardson, M. I. (2015). The origin, evolution, and trajectory of large dust storms on Mars during Mars years 24–30 (1999–2011). *Icarus*, *251*, 112–127. https://doi.org/10.1016/j.icarus.2013.10.033

Whelley, P. L., & Greeley, R. (2006). Latitudinal dependency in dust devil activity on Mars. *Journal of Geophysical Research*, *111*(E10), E10003. https://doi.org/10.1029/2006JE002677

Wilson, R. J. (1997). A general circulation model simulation of the Martian polar warming. *Geophysical Research Letters*, *24*(2), 123–126. https://doi.org/10.1029/96GL03814

Wu, Z., Richardson, M. I., Zhang, X., Cui, J., Heavens, N. G., Lee, C., Li, T., Lian, Y., Newman, C. E., Soto, A., Temel, O., Toigo, A. D., & Witek, M. (2021). Large Eddy Simulations of the Dusty Martian Convective Boundary Layer with MarsWRF. *Journal of Geophysical Research: Planets*, *126*(E9), 612-623. https://doi.org/10.1029/2020JE006752

Zurek, R. W., & Martin, L. J. (1993). Interannual variability of planet-encircling dust storms on Mars. *Journal of Geophysical Research: Planets*, *98*(E2), 3247–3259. https://doi.org/10.1029/92JE02936

UAE UNIVERSITY MASTER THESIS NO. 2022:53

This thesis studied the phenomena of global dust storm events (GDEs) on Mars using the model MarsWRF. It is designed to simulate the Martian atmosphere for many Martian years (MYs). One major problem is to set up MarsWRF to Produce GDEs in a few MYs, but not in others. This first chapter will introduce the Mars atmosphere, the dust cycle and previous relevant literature. The second chapter discusses the model MarsWRF and how it works. Finally, the last chapter shows the result for the optimal model run and its comparison with higher resolution model runs.

Khulood Alshehhi received her Master of Science Physics from the Department of physics, College of Science and her Bachelor of Science in Physics from the College of Science, UAE University, United Arab Emirates.

www.uaeu.ac.ae